1 <u>**Supplementary Information**</u>

2 **Northern Hemisphere atmospheric history of carbon monoxide since**

3 **preindustrial times reconstructed from multiple Greenland ice cores**

4 **Xavier Faïn et al. (2021), Climate of the Past**

5 ## Summary

28

1. Methodology
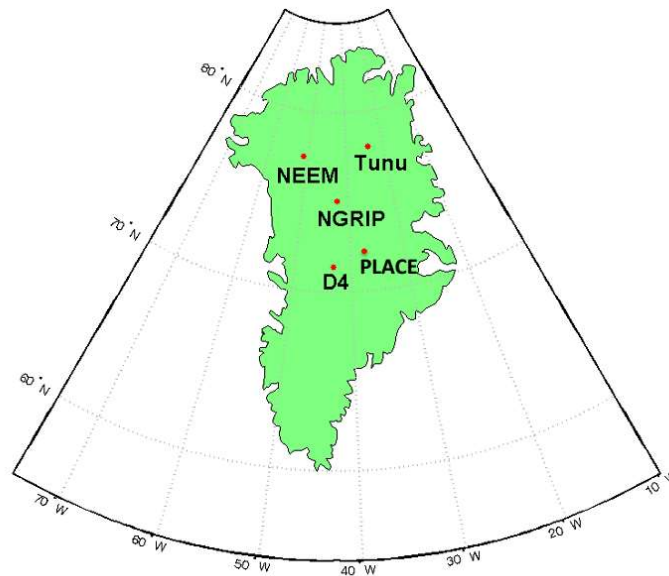
1.1. Location of drillings

Figure S1. Drilling locations of the ice cores featured in this study: NEEM, Tunu13, NGRIP, D4, PLACE. These sites are all located within Greenland.

1.2. Ice core chronologies

Ice core	Δage (yrs)	FWHM (yrs)	Ice Age Scale	Gas Age Scale
D4	90	14	ALC+VS Gas	Tied to WDC06A-7[b] & Law Dome[c]
Tunu13	314-369	21-27	ALC+Vs[d]	Tied to WDC06A-7[b]
NGRIP	235	18	Ice: GICC05[e]	Tied to WDC06A-7[b]
PLACE	195	n.d.	ALC+VS	Tied to WDC06A-7[b]
NEEM-SC	187[a]	17	Ice: GICC05[e]	Gas: GICC05[e]
NEEM-2011-S1	187[a]	17	Ice: GICC05[e]	Gas: GICC05[e]

Notes: Δage=difference between gas age and ice age. If no reference is provided, value is estimated by age scale synchronisation; FWHM=Full Width at Half Maximum of gas age distribution at close-off depth estimated by OSU firn air model (Rosen et al., 2014); ALC=annual layer count; VS=volcanic synchronisation; gas age scales do not incorporate lock-in zone measurements. [a] Buizert et al. (2014); [b] Mitchell et al. (2013); [c] MacFarling Meure et al. (2006); [d] Sigl et al. (2015); [e] Rasmussen et al. (2013).

Table S1. Information on ice and gas age scales for the ice cores featured in this study

1.2. Differences and similarities between DRI and IGE CFA setups

Specific details of analytical setups are reported in Table S2. Small operational differences exist between the laboratory setups at DRI and IGE. First, DRI and IGE melter geometries are different, and described by McConnell et al. (2002) for DRI, and Bigler et al. (2011) for IGE. Second, the melting rate was higher at DRI compared to IGE ([5-6] cm min^{-1} and 4 cm min^{-1}, respectively). Finally, DRI and IGE debubblers have different geometry. DRI debubbler (Plexiglas-made) allows for ultra-high resolution of liquid phase analyses, but results in a larger mixing of the gas phase sample compared to the IGE debubbler (glass-made) specifically designed for gas measurement.

The same optical feedback cavity enhanced absorption spectrometer was used to analyse carbon monoxide and methane at both DRI and IGE and during the all analytical campaigns (2013, 2015, and 2017). The same instrument was used by Faïn et al. (2014) for measurements of the NEEM-2011-S1 core in 2011 at DRI.

Two different gas extraction units were used (i) in 2013 (DRI), and (ii) both in 2015 at DRI and 2017 at IGE, respectively. A gas extraction unit includes a degasser, a pressure transducer, a 6-ways valve, and a homemade Nafion dryer (Fig.1 of Rhodes et al., 2013). Improvements on the design and operation of this unit largely explain the improved stability of the [CO] CFA signal, as shown by the much larger optimal IT values observed for the 2015 and 2017 campaigns (Table S2).

Finally, the D4, Tunu13, and a fraction of the NEEM-SC cores were analysed with a Micromodule 0.5×1 degasser (Membrana GmbH, Germany). Other cores were analyzed with an Idex Transfer-Line degasser instead.

Ice core	Laboratory of analysis	Analysis date	Depth Interval (m)	Mean melting rate (cm min-1)	Mean gas sample flow (sccm min-1)	Melter head	Degasser	Optimal Integration Time (s)	Integration Time applied (s)	Internal precision at IT (ppbv) (2σ)	External precision (ppbv)	System response time (min)	CO blank (ppbv)	CO solubility losses (%)
Tunu13	DRI	13-21/08/13	213–73	5.9	1.8	Standard	M	130	6	1.4	5.7	15	35±7	3.7%
D4	DRI	7-9/08/13	146–61	7.6	1.5	Small	M	130	6	1.4	5.7	15	35±7	3.7%
		15/08/2013	145–123	7.6	1.5	Small	M	130	6	1.4	5.7	15	35±7	3.7%
NEEM-SC	DRI	3-6/09/13	573–491, 444–399	5.7	1.9	Standard	M	130	6	1.4	5.7	15	35±7	3.7%
		7-8/10/13	491–444	5.7	1.8	Standard	IL	130	6	1.4	6.6	14.2	12.6±4.4	6.0%
NGRIP	DRI	08/31/13	91–74			Standard	IL	130	6	1.4	6.6	14.2	12.6±4.4	6.0%
		30/09-4/10/13	254–207, 108–91, 569–519	5.7	1.4	Dual ring	IL	130	6	1.4		14.2	12.6±4.4	6.0%
PLACE	DRI	28/09-01/10/15	153 - 80	5.4	1.6	Standard	IL	>500	1	1.6	6.6	9.3	7.4±1.4	6.4%
PLACE	IGE	31/01-10/02/17	153 - 80	4.0	1.4	Bigler et al., 2011	IL	>1000	1	1.2	3.3	1.6	4.1±1.2	8.8%

Degasser: M=Membrana Liqui-cel Micromodule; IL=Idex Transfer Line degasser.

Melter head; three different styles were used: standard = as McConnell et al. (2002); small = smaller cross-sectional area; dual ring = new design with two concentric sample rings available for gas

1

2 **Table S2.** CFA setup specifications and performances of the different analytical campaigns.

1.3. Calibration of SARA analyser

The optical response of OF-CEAS (based on absorption) to gaseous concentrations of samples circulating in the cavity of the spectrometer is highly linear (Morville 2005). Such linearity has been previously reported for concentrations ranging over more than three decades for methane (e.g., Fourteau et al., 2017).

Similarly, we observed a highly linear relationship of our OF-CEAS spectrometer when measuring CO mixing ratios over a [0-100 ppbv] range. Such linearity was demonstrated by a dilution experiment conducted by mixing a 100 ppbv standard gases and CO - Air Zero with two MFC MKS recently calibrated (concentrations ranging [0-100] ppbv could thus be generated). Fig. S2 reports uncalibrated SARA [CO] plotted along expected [CO] based on dilution flows, with a negligible offset and a 0.92 slope. Recent laboratory measurements have extended the observation of the OF-CEAS linearity at CO concentrations of 2.7 ppmv (R. Grilli, pers. com.).
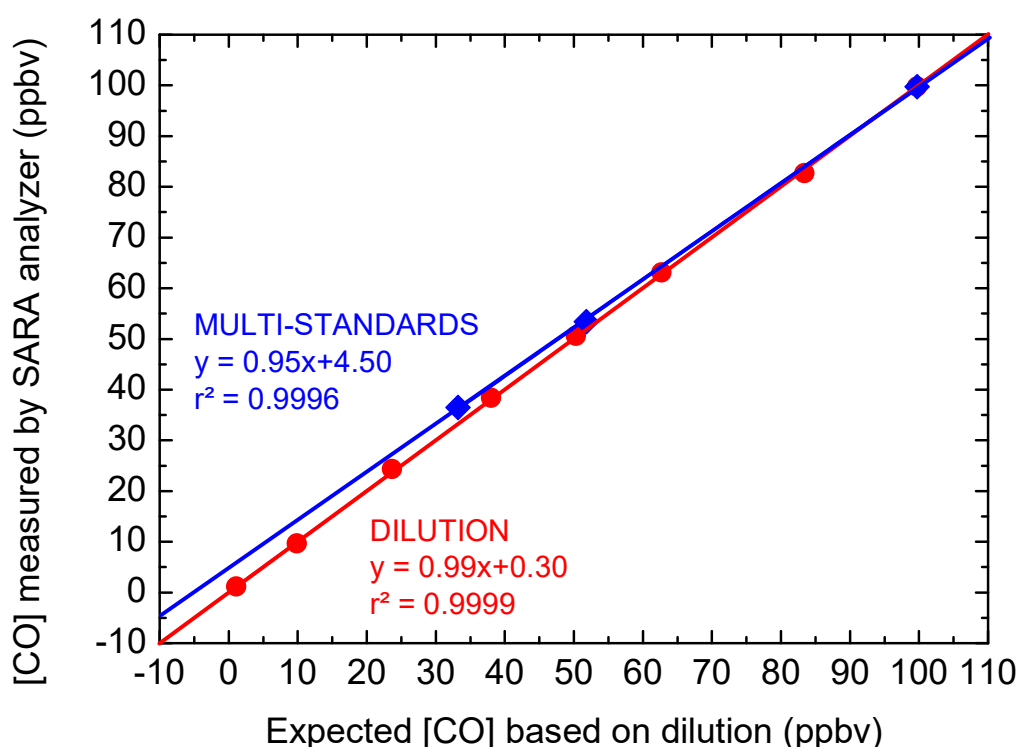

Figure S2. Calibrations of the OF-CEAS SARA analyzer for CO. (i) multi-standard calibrations (blue dots): uncalibrated SARA CO is plotted along with NOAA WMO_2014 CO concentrations from three standard gases. (ii) a dilution experiment conducted by mixing a 100 ppbv standard gas and CO-Air Zero with two mass flow controllers: uncalibrated SARA [CO] is plotted along with expected [CO] based on dilution flows.

5

1 For each analytical campaign, the OF-CEAS spectrometer was carefully calibrated on dry gas by
2 direct injection of a synthetic standard gas (Scott Marin, artificial gas mixtures) precisely calibrated
3 onto the NOAA/WMO X2014 scale, with a concentration close or above 100 ppbv (Table S3).
4 Knowing the excellent linearity of the instrument, a calibration factor was established as the ratio
5 of the NOAA-certified and the measured CO concentrations for this single standard gas. This is
6 consistent with the fact that the zero of the spectral measurements is intrinsically accurate.

Analytical campaign	Gas Cylinder used for OF-CEAS (SARA) calibration	Gas Cylinders used for CFA calibration	NOAA certified [CO] (ppbv)
DRI 2013		CA04382	56.6 ± 3.4
		CA04332	97.2 ± 0.0
	CC302559	CC302559	142.6 ± 0.1
DRI 2015		CB10010	57.9 ± 0.4
	CA04332	CA04332	97.2 ± 0.1
DRI 2013		CB09754	32.5 ± 0.1
		CB09722	51.7 ± 0.1
	CB09752	CB09752	100.1 ± 0.1

8 **Table S3.** Synthetic standard gases (Scott Marin, artificial gas mixtures) precisely calibrated onto the
9 NOAA/WMO X2014 scale and used for OF-CEAS and CFA calibrations.

10

1.4. Determination of CO CFA blank

12 Excellent agreement between replicate measurements conducted days apart, before blank
13 correction, suggests that CO blanks of gas-CFA analytical systems (both DRI and IGE) can be
14 very constant during an analytical campaign (Fig. S3; see Fig. 2 of Faïn et al., 2014). However,
15 how to quantify exactly such procedural blanks remains complex. Two approaches investigate
16 gas-CFA procedural blanks: single-standard measurements, or multi-standards calibration.

17 To evaluate CO blank with single-standard measurements approach, deionized (DI) water is
18 bubbled with a specific gas standard for at least 12 hours in a 2 liters reservoir, and this water is
19 later mixed with the same gas standard in the calibration loop (CL, section 2.2.2 of manuscript).
20 The positive offset between direct measurements of the dry gas standard with the spectrometer
21 and the CL measurements as described previously will directly indicate the procedural blank.
22 Single-standard measurements were conducted to evaluate CO blank of the IGE CFA setup. An
23 example of such experiment is as follow: DI water bubbled during 18 hours with a 58.7±0.3 ppbv
24 (NOAA/WMO X2014 scale) CO standard gas. The same standard gas was then mixed with this

6

1 DI water within the IGE calibration Loop, and circulated toward the degasser. CO mixing ratios of

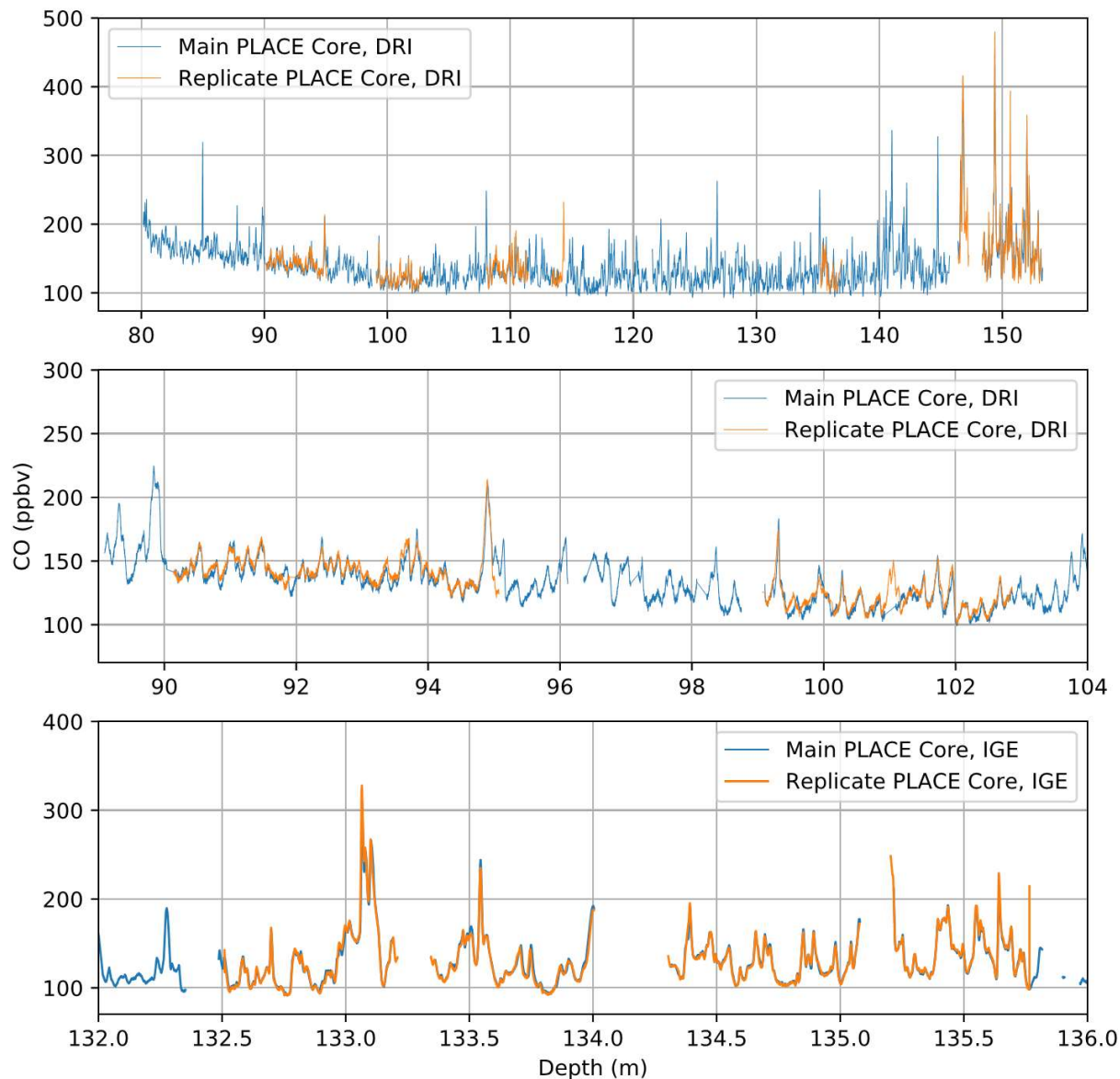2 62.8±0.5 ppbv is measured. A procedural CO blank of 4.1±0.6 ppbv is thus observed.

4 **Figure S3.** Replicate measurements of CO mixing ratios (Main cuts blue, Replicate cuts in orange)

5 conducted on the PLACE core (i) at DRI during the 2015 analytical campaign (upper and middle panels),

6 and (ii) at IGE during the 2017 analytical campaign (lower panel).

7

8 Multi-standard calibration loop datasets have been widely used before for methane (e.g., Rhodes

9 et al., 2016; Fourteau et al., 2017) and are obtained by mixing a range of standard gases of known

1 concentration with He-degassed DI water. The intercept observed when plotting expected versus

2 CL-determined concentrations reflects both the procedural blank and the fraction of gas remaining

3 in DI water after He-bubbling. Figure S4 reports multi-standards CO calibration obtained at DRI

4 in 2013 with both Micromodule and Transfer Line degassers, and the intercepts of 35 ppbv and

5 12.6 ppbv are the CO blank levels observed for these two specific CFA configurations. We applied

6 the multi-standards calibrations loop approach to evaluate CO blank for all continuous CO

7 datasets collected in this study (Table S2). At IGE, the multi-standards calibration provided an

8 Intercept for [CO] of 4.1 ppbv, in good agreement with the single-standard approach described

9 before. This good agreement demonstrates that the multi-standards calibration is a reliable

10 approach to evaluate CFA blank for gas of low solubility such as CO, i.e. the fraction of CO

11 remaining in DI water after He-bubbling is negligible. Estimation of the uncertainty of CO blanks

12 are reported on Table S2 and are based on repeated calibration loop measurements throughout
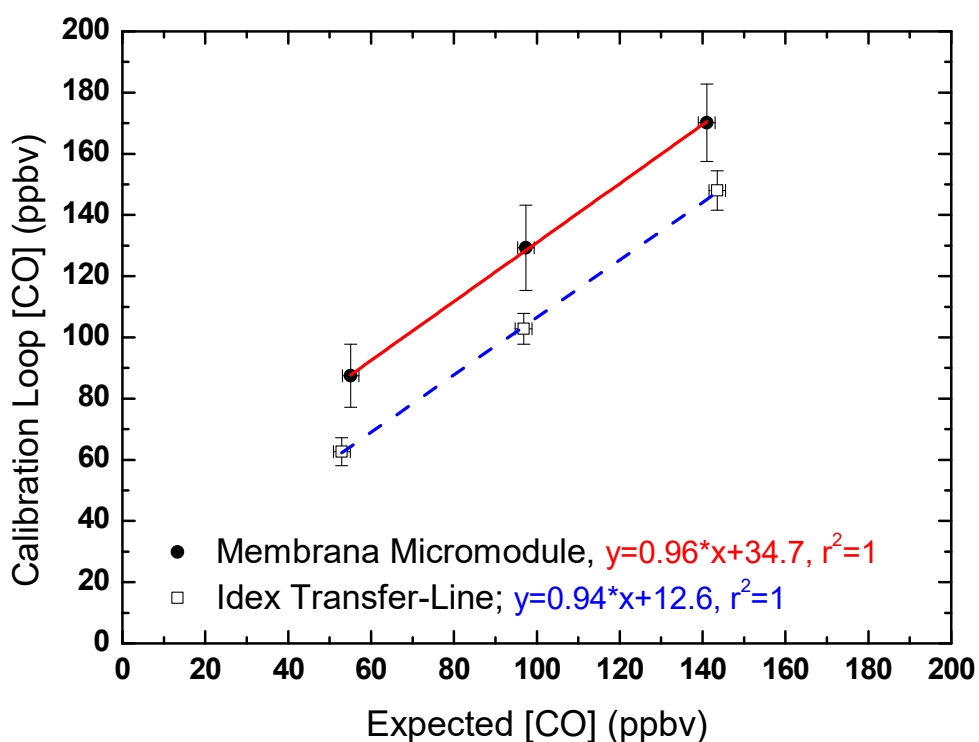
13 the campaigns (1σ).

14

15 **Figure S4.** Multi-standards CO calibrations conducted at DRI in 2013 with both Micromodule and Transfer-

16 Line degassers.

17

1 Overall, using a Membrana MicroModule degasser results in larger CO blank, and we
2 consequently recommend the use of Idex Transfer-Line degassers for continuous CO analyses.
3 Also, any material (e.g., line, connections) should be carefully tested to assess potential CO
4 contamination. We have found that TEFZL is appropriate for CO analyses. Finally, CO blanks are
5 kept low by continuously running DI water through system lines during measurements periods.

6

1.5. Internal precision of CO CFA analyses

8 Internal precision and stability of gas-CFA measurements were evaluated by Allan variance tests
9 (Allan, 1966) applied to calibration loop dataset (DI degassed water mixed with a single standard
10 gas), and are reported on Fig. S5. Observed optimal integration times (i.e., time of lowest Allan
11 deviation) were 130 sec for the 2013 DRI campaign, larger than 500 sec for the 2015 DRI
12 campaign, and larger than 1000 sec for the IGE 2017 campaign. For the 2015 and 2017
13 campaigns, the design of the calibration loop (specifically, the volume of degassed water available
14 combined with the setup sample flow rate reproduce during calibration loop experiment) did not
15 allow a minimum in Allan Variance to be reached, but still provided an upper bound value.

16 To maximize the depth resolution, gas data are averaged over integration time (IT). Such
17 integration time was set up to 6 sec for the 2013 DRI campaign (Tunu13, D4, NGRIP, and NEEM-
18 SC ice cores), and 1 sec for the 2015 DRI and 2017 IGE campaigns (ice core : Place). The internal
19 precision (2σ) can be defined as twice the Allan deviation at these chosen integration times,
20 resulting in an internal precision of [CO] of 1.4 ppbv, 1.6 ppbv, 1.2 ppbv for the analytical
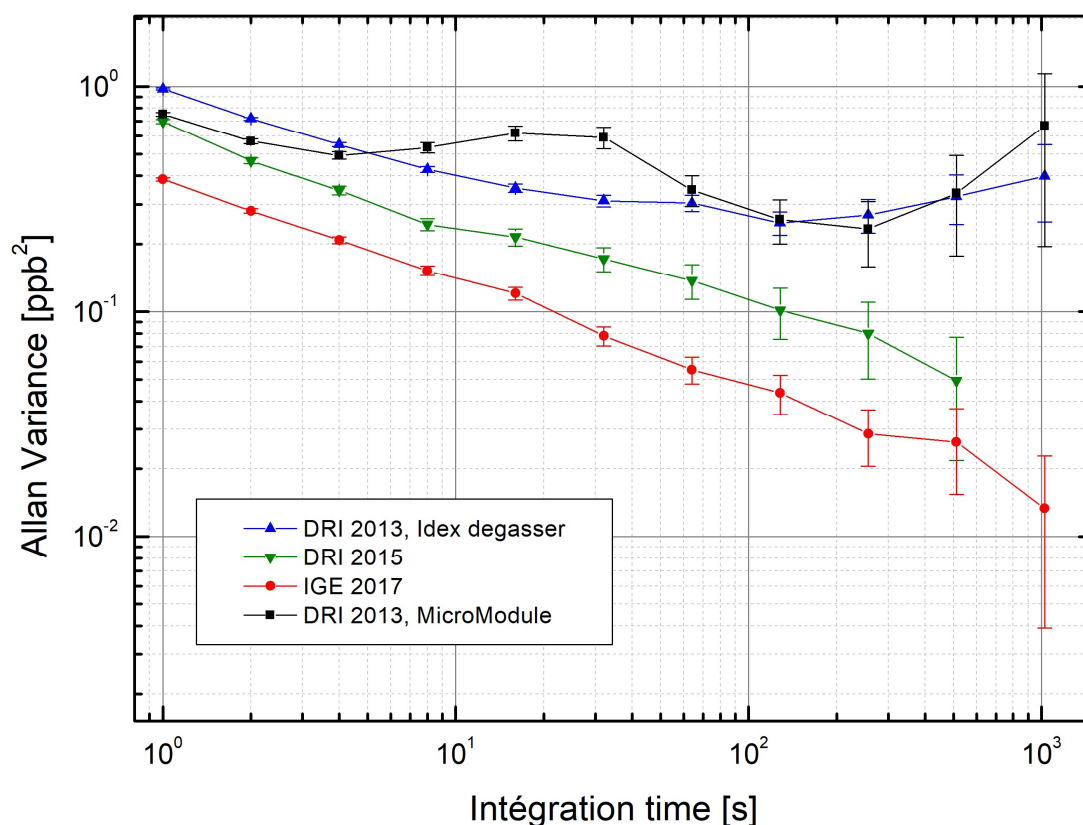21 campaigns 2013-DRI, 2015-DRI, and 2017-IGE respectively.

Figure S5. Allan variance results for calibration loop dataset (DI degassed water mixed with a single standard gas) collected for the different CFA setup: DRI 2013 (both Transfer Line and Mircomodule degassers), DRI 2015, and IGE 2017.

1.6. External precision of CO CFA analyses

External precision of the continuous CO measurements (i.e., including all sources of errors or bias) can be investigated by melting replicate ice sticks on different days on a gas-CFA setup. Specifically, we define the external precision as the pooled standard deviations calculated on the differences of CO concentrations from main and replicate analysed ice sticks, averaging continuous CO data over few cm long intervals.

For the DRI gas-CFA setup, an external precision of 5.7 ppbv can be extracted from a 18m long replicate section of the NEEM-2011-S1 core analyzed in 2011 (Faïn et al., 2014), averaged over 9 cm long intervals. In this study, we use this estimate of external precision to datasets collected at DRI in 2013, with a Micromodule degasser (i.e., D4, Tunu13, a fraction of NEEM-SC).

10

1   Similar characterizations were conducted during the 2015 DRI and 2017 IGE analytical

2   campaigns by melting replicate sticks from the PLACE core, taking advantage of the large amount

3   of ice available (the PLACE core is 27 cm diameter, drilled with the Blue Ice Drill, see sect. 2.1 of

4   manuscript). 19.6 m (resp. 2.3 m) of replicate PLACE sticks were analysed at DRI in 2015 (at

5   IGE in 2017, resp.). Replicate sections of the PLACE core melted both at DRI and IGE are

6   reported on Fig. S3. CO concentrations measured on both main and replicate ice sticks were

7   averaged by binning over 196 10-cm long (resp., over 227 1-cm long) intervals at DRI (resp., at

8   IGE). Figure S6 reports an excellent correlation ($r2 = 0.99$; $p<0.01$) between averaged CO from

9   main cuts versus averaged CO from replicate cuts for both CFA setup. Finally, external precision

10   of 6.6 ppbv (resp., 3.3 ppbv) was calculated for the 2015 DRI campaign (resp., 2017 IGE

11   campaign). In this study, we apply the external precision value established for the 2015 DRI

12   campaign is applied to dataset collected at DRI in 2013 with a Transfer-Line degasser (i.e., a

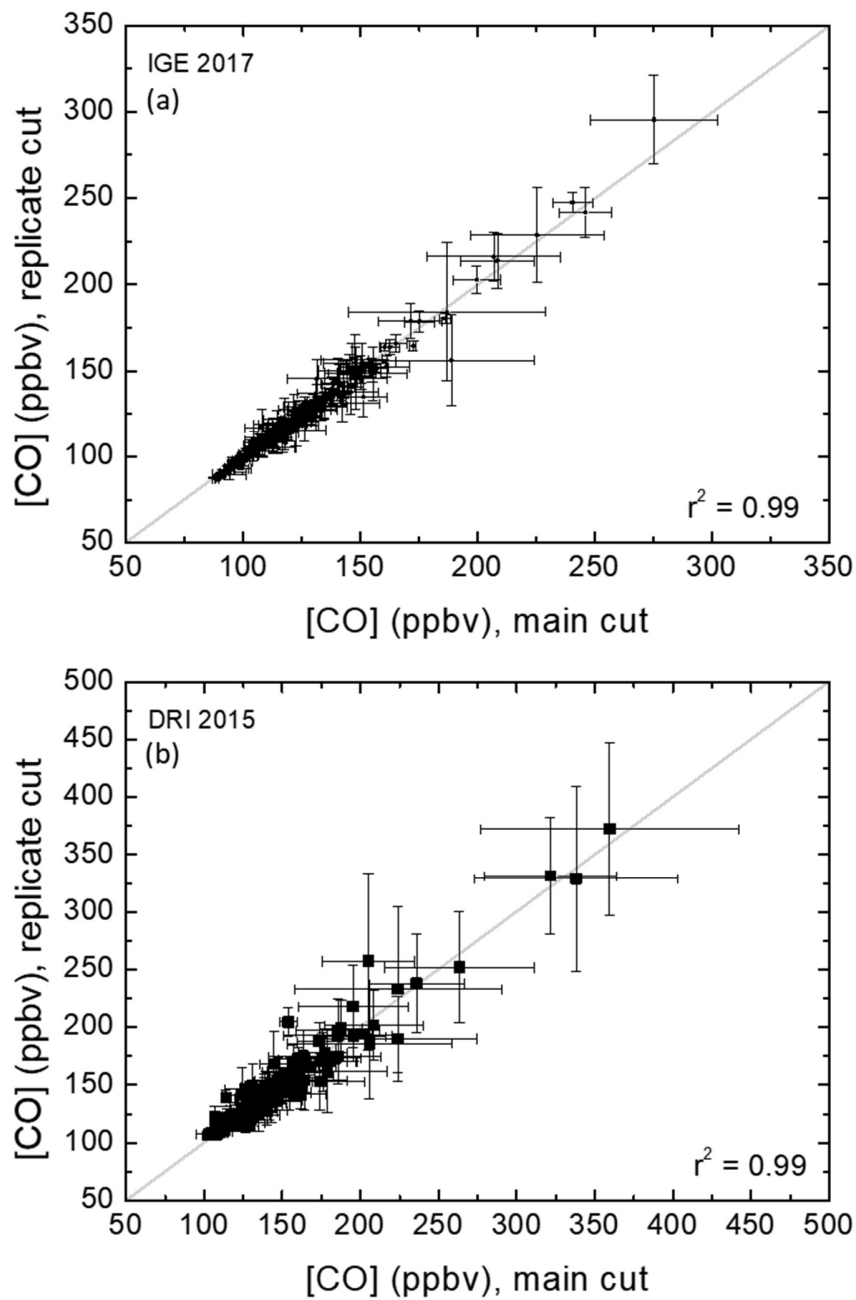13   fraction of NEEM-SC and NGRIP dataset).

14

Figure S6. CO mixing ratios measured on both main and replicate PLACE ice sticks at DRI (a) and IGE (b), after averaging data over 10-cm long (resp., over 1-cm long) intervals at DRI (resp., at IGE).

We are aware that longer replicate sections, spanning depths over the entire record, such as conducted at DRI in 2015 (Fig. S3), can provide a more solid dataset for evaluating external precision. We note that only the DRI PLACE dataset was used to extract atmospheric information

1 (section 3 of manuscript), notably because a more robust evaluation of the external precision was

2 available. However, the IGE dataset demonstrates that excellent precision of continuous CO

3 measurements is not limited to one specific setup, but rather achievable for all CFA laboratories.

4

1.7. Internal CO CFA calibration: improving accuracy

6 A fraction, or all, of gases dissolved in the water CFA sample flow are not recovered by the

7 degassers used in this study. CO solubility is higher than N2 or O2 solubility. This preferential

8 dissolution of CO in comparison to N2 and O2 results in underestimated CO mixing ratios when

9 detected at the gas outlet of the degasser. This underestimation of CO mixing ratios need to be

10 accurately quantified so as to provide an absolute calibration of CO continuous dataset. Henry's

11 Law theory suggests that temperature and gas/liquid ratio of the melted sample are two important

12 parameters influencing gas dissolution within the sample flow. Gas/liquid ratio of the melted

13 sample is likely related to the air content of the ice analysed, although this relationship may not

14 be straightforward (e.g., one cannot exclude losses of gas at the melter), and may differ with

15 melter geometry.

1.7.1. Rationale for an internal CFA calibration

17 In this study, we use the calibration loop so as to calibrate internally (i.e., with CFA data)

18 continuous CO datasets. This choice relies on the following observations:

19 ● The amount of gas dissolved in the water stream and not recovered by the degasser (Idex

20 Transfer-Line or Membrana Micromodule) is dependent on the CFA setup, i.e. dependent

21 on its geometry, components, operation. Consequently, a unique theoretical framework

22 cannot be applied to all dataset. Indeed, in this study a 73 m long ice core (PLACE) was

23 analysed on two different CFA setups (at IGE and DRI), for CO but also for methane

24 mixing ratios. This gas CFA laboratory intercomparison revealed that the fraction of

25 methane not recovered at IGE was larger than a DRI (10% and 13%, resp.). The gas

26 extraction unit (including an Idex Transfer-line degasser) and OFCEAS detection were

27 identical at DRI and IGE, pointing out that the melter and lines upstream the degasser can

28 result in different gas dissolution ratios.

29 ● To test further the influence of the CFA setup geometry and operation on gas dissolution

30 patterns, a series of 16 replicate 1m long ice sticks, all cut from the same Blue Ice Drill

31 (BID) large diameter core recovered in the vicinity of Greenland summit (C14 camp, Hmiel

et al., 2020), were melted at IGE in December, 2018, with varying operation and geometry of the CFA setup. Each time, the fraction of methane not recovered was observed. Specifically, the influence of following parameters on the preferential methane dissolution were tested: melting speed (varying from 2.8 to 6 cm min^{-1}), sample flow (ranging 12 to 22 ml min^{-1}), melter geometry (geometry reported by Bigler et al., 2011, with inner sections of 26 x 26 mm, or 24 x 24 mm), line lengths (adding 4 m long line sections in the system). These tests are specific to the IGE setup, but they show: (i) no influence of the melting speed, neither of the melter geometry, neither of the sample flow, on the preferential methane dissolution. However, they reveal varying methane losses when changing line geometry (up to 5% in mixing ratio).

Overall, these results show that CFA setups are dynamic systems, not at solubility equilibrium.

1.7.2. Principle of calibration

We hypothesize that CO and methane dissolution follow the same physical laws: consequently, if a calibration loop (CL) is able to reproduce methane preferential dissolution, it should also reproduce CO losses related to dissolution. Calibration loop is described in sections 2.2.2 of manuscript and 1.4 of SI; briefly, a 10:90 mixture of synthetic air and degassed deionized (DI) water can be introduced into the system via a 4-port valve located directly after the melterhead. The water is sourced from a 2 L reservoir degassed by constantly bubbling ultra-pure helium through it, and the fraction of He dissolved in DI water is later neglected. The air–water mixture follows the same path through the system as the ice core sample before being analysed by the laser spectrometer. We verified that no CO or CH4 specific fractionations occur at the degasser, which would invalidate the previous hypothesis. To do so, we run consecutively the calibration loop in two configurations: (i) with a degasser, and (ii) with an open split debubbler where gases are transferred to the OF-CEAS analyzer without going through a membrane. Same CH4 and CO mixing ratios were observed in both configurations. Finally, considering that gas dissolution within the CFA setup is likely to vary with ice air content (AC), we tried to determine a specific calibration for each ice core analyzed.

We first needed an estimation of methane losses related to dissolution, independent of the calibration loop, from each ice core analyzed. For the archives Tunu13, D4 and NEEM, preferential methane dissolution was already known (Rhodes et al., 2013, 2016). For the PLACE and NGRIP archives, it was evaluated by direct comparison of CFA dataset with GISP2 discrete record (Mitchell et al., 2013).

1 Then, liquid and gas flows injected through the calibration loop were chosen to reproduce ice AC

2 value. We operated the calibration loop with different artificial gas cylinders of known CO and

3 CH4 mixing ratios. Reference and CO mixing ratios of these cylinders are reported in Table S3.

4 Gas flow injected through the calibration loop was later adjusted if required so as the calibration

5 loop reproduces nicely the expected methane preferential dissolution. We note that such

6 adjustments were more pronounced at IGE than at DRI, showing that the geometry of the

7 calibration loop itself can also impact how gas dissolves within the CFA setup.

8 After and/or before each calibration loop experiment, gas from all cylinders were analysed directly

9 with the OF-CEAS analyser. We know that the internal calibration of the SARA analyser is very

10 stable with drift over periods of time of few hours. The Calibration Loop data were not calibrated

11 onto the NOAA/WMO X2014 scale, but instead directly compared to these "dry" measurements.

12 **1.7.3. Calibration parameters**

13 Each continuous CO dataset, after initial calibration of the OF-CEAS analyser (Sect. 1.2), was

14 calibrated using multi-standards calibration loop dataset. As an example, Fig S4 reports the multi-

15 standards calibration loop dataset obtained for the 2013 DRI analytical campaign (with two

16 degasser configurations). The following can be extracted from such calibration datasets:

17 $[CO]_{COR} = ([CO]_{SAMPLE} - CO_{BLANK}) / SC$

18 With CO_{BLANK}, the CO blank of the CFA setup determined for each analytical campaign (Sect. SI

19 1.4), and SC the Solubility Correction evaluated with CL experiment (Sect SI 1.7.2). Table S2

20 reports SC (and CO blank) for each ice core analysed. The lowest SC, i.e. 3.7%, was observed

21 during the DRI 2013 campaign, when using a Membrana Micromodule degasser. The SC

22 observed when using an Idex Transfer-Line degasser ranged [6.0-8.8]%; this limited SC range

23 includes 3 different CFA configurations (DRI 2013, DRI 2015, and IGE 2017).

24 **1.7.4. Evaluating Internal CFA calibration**

25 CO has a low solubility, and SC observed were always below 10%. However, our internal CO

26 CFA calibration had to be evaluated. To do so, five 986 g discrete samples from the PLACE core

27 were analysed at UR, following a modified version of the protocol detailed on Sect. SI 1.9 in which

28 the ice samples are not grated into a powder and standard gas is not added to the vessel before

29 melting the sample. [CO] obtained from these discrete measurements can be compared to the

30 continuous CFA dataset, collected at both DRI (2015) and IGE (2017). Only five samples were

31 analysed discreetly, as this analytical capability was designed only in late 2019, and applied in

1   priority to investigate if high frequency CO spikes observed in Greenland continuous CO records

2   could be driven by in-extractu, production as described in Sect. 3.2.5 (in-extractu CO production

3   occurs during the melting analytical process). However, the depths of the five discrete samples

4   described here ranged the entire core, from 84 to 146 m depth.

5   A direct comparison of discrete and continuous dataset is reported on Fig. S7. The standard

6   deviation of the differences between discrete and CFA-based CO measurements is 1.8 ppbv and

7   2.8 ppbv for the IGE (n=5) and DRI (n=4), respectively. The average offset between discrete and

8   CFA-based CO measurements is 1.3 ppbv and 2.1 ppbv for the IGE (n=5) and DRI (n=4),

9   respectively. This excellent agreement supports our approach to internally calibrate continuous

10   CO, and demonstrates that continuous [CO] dataset can now be accurate, which is an important

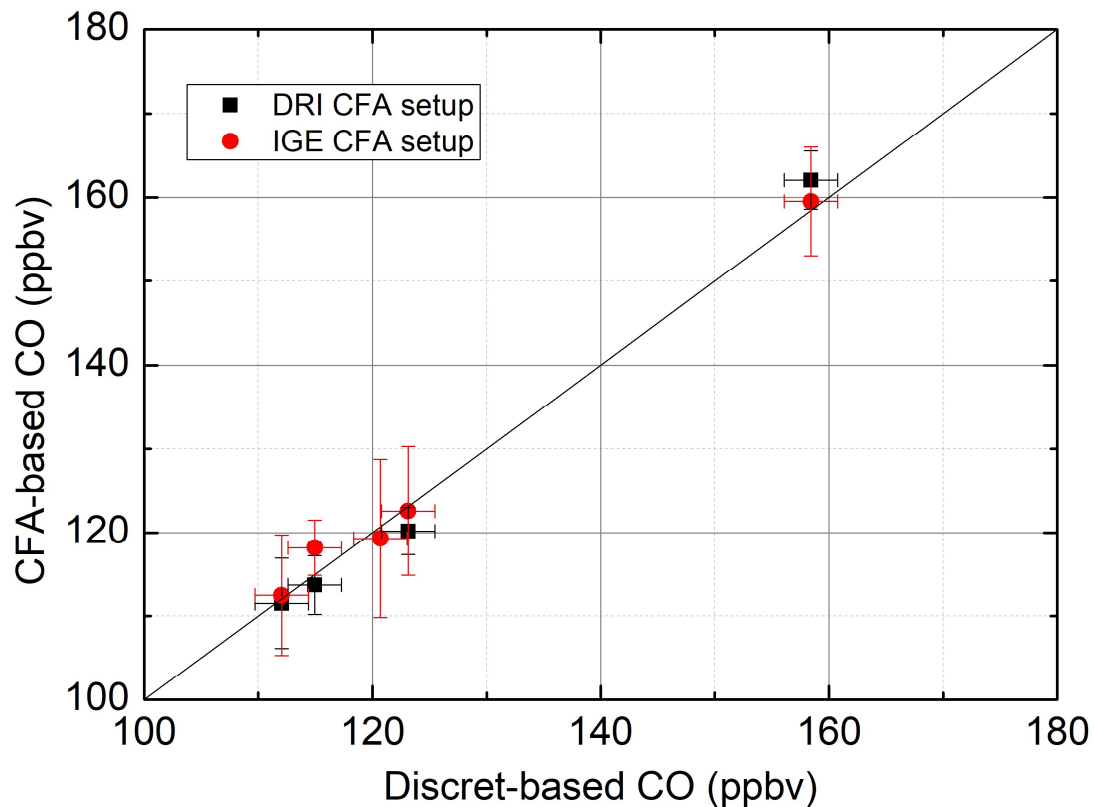11   improvement since the NEEM-2011-S1 measurements (Faïn et al., 2014).

13   **Figure S7.** Comparison of CO mixing ratios measured on the PLACE ice core by discrete or continuous

14   methods. Discrete dataset is compared with both DRI and IGE continuous CO dataset. Sample depth

15   intervals encompassed the entire span of the PLACE core, from 84 to 146 m depth.

1   **1.8. Smoothing of continuous CO measurements**

2   Due to mixing and dead volumes, the CFA system introduces a smoothing of the gas signals.

3   Using the method described in Stowasser et al. (2012), we measured during each analytical

4   campaign the switch between two mixes of deionized water and standard gases (Fig. S8-11, left

5   panels). It allowed us to determine step responses of the CFA systems, which is not instantaneous

6   but spreads over time. During the 2013 DRI campaign, both Idex Transfer-Line and Membrana

7   Micromodule degassers were used (Table S2), and step responses were determined for each
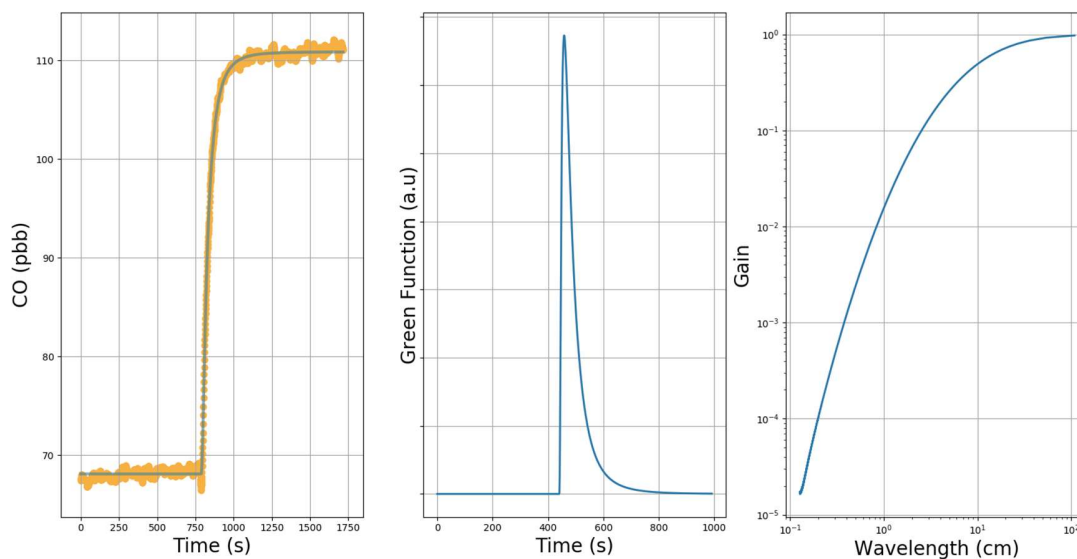
8   degasser configuration.

9

10   **Figure S8.** Left panel: step response of the DRI CFA system operated with a Micromodule (Membrana)

11   degasser in 2013 for analyzing the Tunu13, D4, and NEEM-SC ice cores. Orange dots: measurement

12   points. In blue: fit by the cumulative density function of a log-normal law. Middle panel: Green's Function of

13   the CFA system approximated by a log normal law. Right panel: Gain of the CFA system against the

14   wavelength of sine signals. Gray lines correspond to the cut-off wavelength and a 50% attenuation
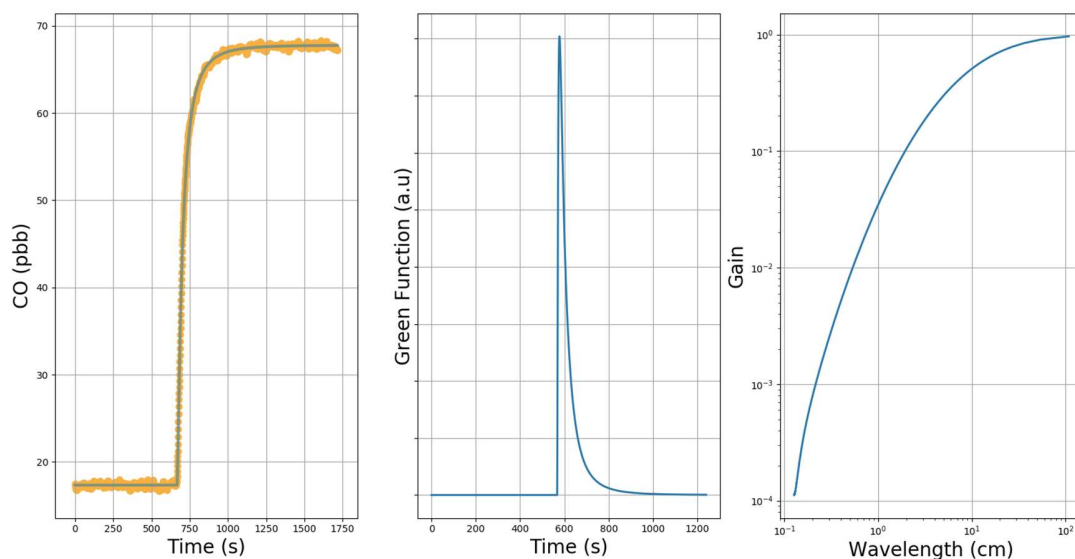
1

Figure S9. Same as Figure S8 for the DRI CFA system operated with a Transfer Line (Idex) degasser in 2013 for analyzing the NEEM-SC and the NGRIP ice cores.
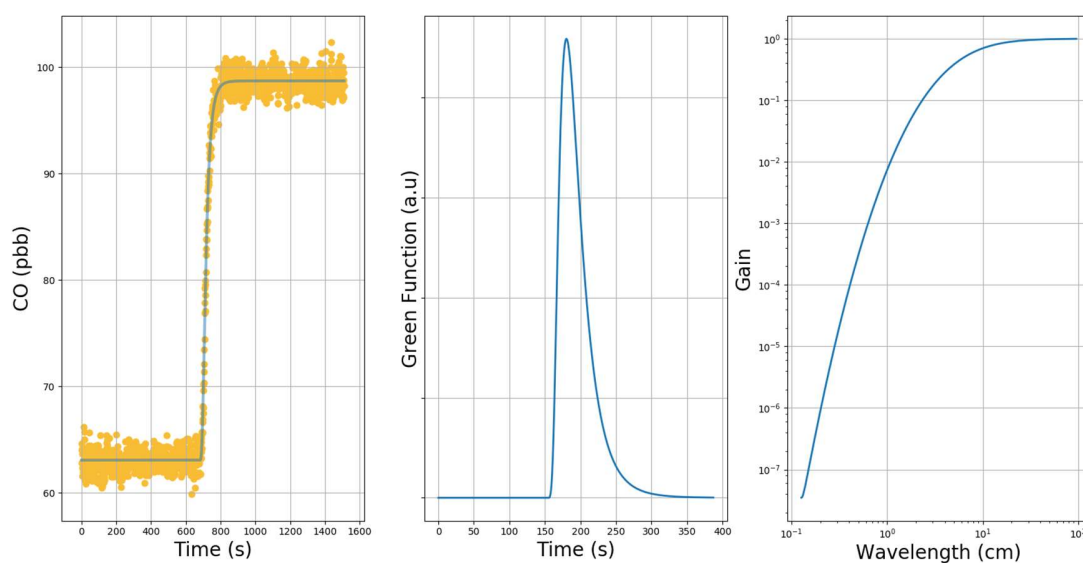
4

5

Figure S10. Same as Figure S8 for the DRI CFA system operated with a Transfer Line (Idex) degasser in 2015 for analyzing the PLACE ice core.
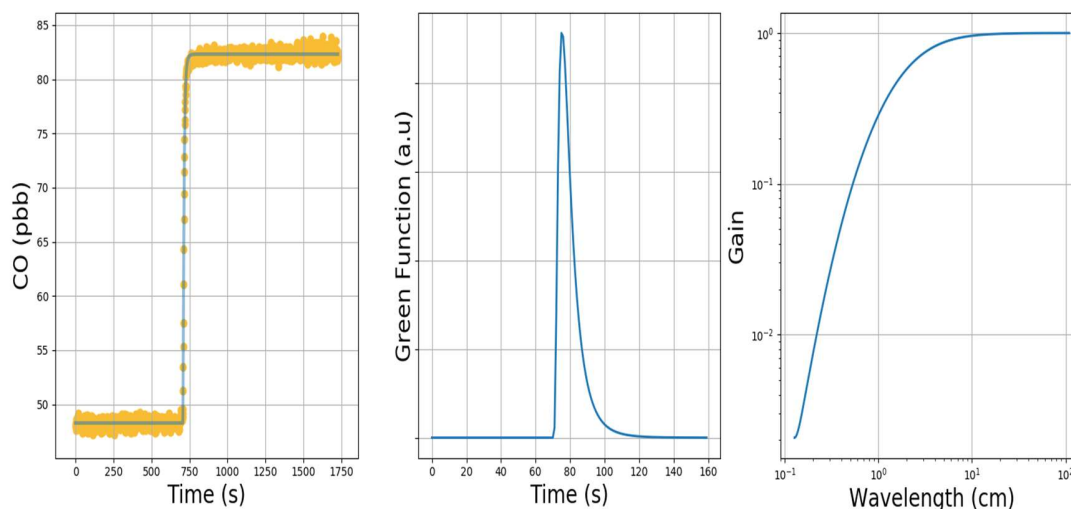
8

18

1

2 **Figure S11.** Same as Figure S8 for the IGE CFA system operated with a Transfer Line (Idex) degasser in

3 2017 for analyzing the PLACE ice core.

4

5 Each observed step response was fitted using the cumulative density function of a log-normal

6 distribution. These log-normal distributions (Fig. S8-11, middle panels) can be considered as the

7 Green's functions, or impulse responses of the CFA systems. Finally, the Green's functions can

8 be used to derive the frequency responses of the systems using Fourier transforms, that is to say

9 the attenuation factors (also referred to as gains) experienced by a sine signal depending on its

10 frequency/period/wavelength. A cut-off wavelength can be defined as the wavelength of a sine

11 signal experiencing a 50% attenuation in amplitude. It is important to note that this cut-off is

12 defined for sine signals, and therefore cannot be directly applied to other types of signals. For

13 instance, Fourteau et al. (2017) reports that a square signal will be less attenuated than a sine

14 signal.

15 During the 2013 DRI campaign, we observed with a melting rate of 5.5 cm min^{-1} cut-off

16 wavelengths of 15.0 cm and 14.2 cm, when using a Micromodule or a Transfer-Line degasser,

17 respectively. A Micromodule was used for the D4, Tunu13, part of NEEM-SC, cores, and a

18 Transfer-Line degasser was used for NGRIP, and a fraction of NEEM-SC (Table S2). During the

19 2015 DRI campaign, we used an Idex Transfer-Line degasser optimized, i.e. shortened to reduce

20 its internal volume to only 1 mL. Consequently, we observed with a melting rate of 5.5 cm min^{-1}

21 a cut-off wavelengths of 9.3 cm. During the 2017 IGE campaign, we used the same shortened

22 Transfer-Line degasser, but the entire gas setup was optimized specifically for gas measurements

23 (including the use of a low dead volume glass debubbler): a cut-off wavelength of 1.6 cm was

19

1 observed. Similar improvements were investigated on the DRI CFA setup in 2015, but could not

2 be fully implemented because they would have decreased the resolution of the liquid phase

3 analyses conducted simultaneously to CO continuous measurements.

4

5 1.8. Impact of storage on CO mixing ratios

6 A 10 m long replicate section of the PLACE core was analyzed nearly two years after the main

7 analytical campaign (respectively December 2018 and February 2017) and no change in the CO

8 values was observed (Fig S12), supporting that CO production in ice during core storage is
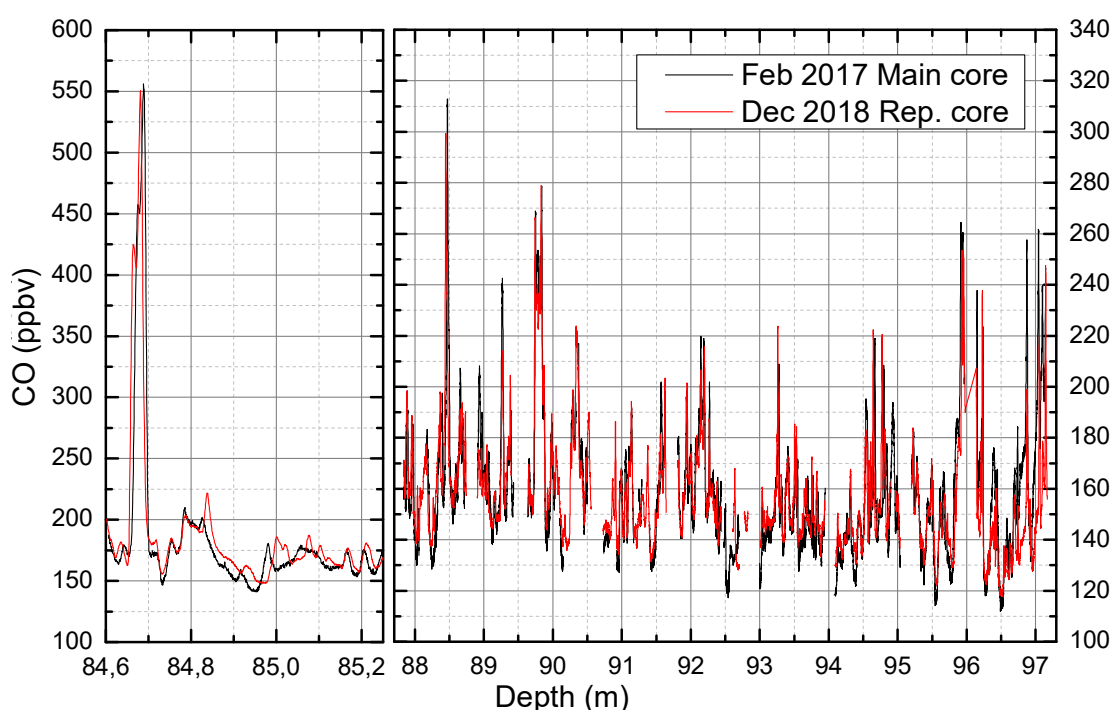
9 unlikely.

11 **Figure S12.** Replicate measurements of CO mixing ratios (Main cuts in black, Replicate cuts in red)
12 conducted on the PLACE core at IGE: replicate sections were analyzed 20 months after the main CFA
13 campaign (in Dec. 2018 and Feb. 2017, respectively).

14

15 1.9. Discrete CO analyses

16 [CO] analyses on discrete ice and firn core samples (including the PLACE core) were carried out

17 at the University of Rochester (UR), with the goals of investigating the possibility of "in-extractu"

18 production of CO during melting of ice core samples from trace organics contained in the ice, as

1 well as to verify that there were no additional uncharacterized artifacts associated with the
2 continuous [CO] method.

1.9.1. Ice Handling and Melting

4 Ice and firn samples are prepared by first removing 0.5 cm of ice from all sides of the sample with
5 a bandsaw using a precleaned blade and solid ceramic bearings. The samples are further cleaned
6 using a stainless steel cheese grater to remove an additional 1-3 mm from all sides. The cleaned
7 samples are placed into a prechilled (-20°C) glass extraction vessel and held in a clean air box
8 flushed with CO-free air. The solid ice (non-firn) samples were grated further to destroy the ice
9 matrix and remove the trapped air. The resulting powder is collected into the extraction vessel.
10 These sample tests are referred to as "Powder Tests".

11 The melting vessel is attached to the air extraction line via a PTFE O-ring that has been
12 continuously flushed with CO-free air to ensure the O-ring will not outgas CO. The extraction
13 vessel is then evacuated, and the integrity of the O-ring seal is verified. A cold bath (-15°C) is
14 applied to the extraction vessel to keep the sample cold and a flow of CO-free air (50sccm) is
15 started to flush the ice sample for at least 12 hours before the sample is run. In addition, a flow of
16 CO-free air (150 sccm) is also flushed around the exterior PTFE O-ring seal to ensure the O-ring
17 does not allow any room CO to diffuse into the extraction vessel during flushing and the
18 extractions.

19 After flushing, the vessel is again evacuated for at least 30 minutes before a known amount of
20 CO standard gas is introduced; the vessel is then isolated from the rest of the system. The sample
21 is melted over ~50 min using a warm water bath maintained at 50°C. The warm water bath is
22 removed while a small amount of ice is still left in the extraction vessel and an ice bath is applied
23 for a minimum of 10 minutes before starting measurements; the ice bath is left on the vessel
24 during the rest of the process.

1.9.2. CO Concentration Measurements

26 The gases in the headspace of the extraction vessel (sample gas) are measured for CO
27 concentration at regular intervals using a reducing gas detector (RGD; Peak Performer 1 from
28 Peak Laboratories). A small aliquot of sample air is expanded into a section of the Pyrex extraction
29 line known as the "Large Volume Loop" (LVL; volume of 155 scc) and the expansion pressure is
30 measured. Ultra-High Purity Air (UHP Air) is then admitted into the extraction line at a steady, low
31 flow rate (50 sccm) to ensure laminar flow in the system. This UHP Air serves as a "push" gas,
32 compressing the sample aliquot into the sample loop of the RGD (the RGD is intended for

1 operation with ambient-pressure samples). A simplified schematic of the UR analytical setup

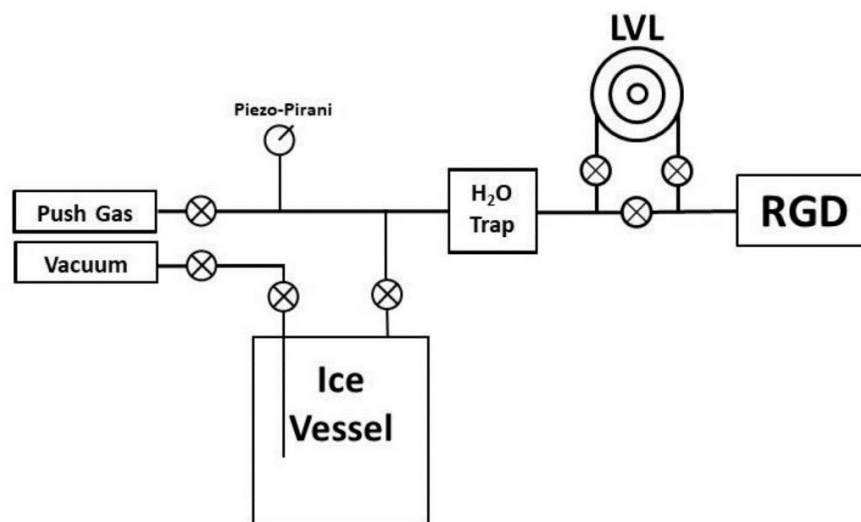2 dedicated to discrete CO measurements is reported on Fig. S13.

3

4 **Figure S13.** A simplified schematic of the expansion volume used for the discrete CO measurements.

5 Sample gas is held in the Ice Vessel and expanded into the "LVL" (Large Volume Loop, ~155 cm^3 volume)

6 and into the "RGD" for measurement. Water vapor is removed by the H$_2$O trap held at ~-60°C with a dry

7 ice and ethanol mixture and the line pressure is monitored with the Piezo-Pirani pressure gauge. The

8 expanded gas is then compressed via a flow of a "push" gas at 50 sccm to ensure laminar flow and prevent

9 rapid mixing with the sample gas. The sample loop in the "RGD" (1 cm^3 volume) is pressurized to 1013

10 mbar for measurement. The sample CO mole fraction is measured by the "'RGD" which is a Peak Performer

11 1 (Model PP1 from Peak Laboratories) Reducing Gas Detector.

12

13 Once the RGD sample loop is pressurized to 760 torr, the sample aliquot is injected and analysed

14 for CO concentration. Between each expansion of sample gas from the extraction vessel, a CO

15 standard is directly measured. This is accomplished by filling the RGD sample loop with a CO

16 standard gas to ambient pressure. The first 20 scc of standard gas is discarded by flushing to

17 either atmosphere or vacuum, after which the standard gas is pressurized (again to 760 torr) and

18 injected. These standard gas measurements allow for the CO concentration of the sample gas to

19 be calculated and for instrumental drift to be corrected for during the tests.

20 Sample gas aliquots are expanded from the vessel several times during the run, to observe the

21 growth of excess CO. All tests are run in a similar manner with similar timings. The first expansion

22 of sample gas from the vessel (Expansion 0) is performed immediately after the standard gas is

22

1 added to the vessel and before melting is started. This expansion is a baseline check of the

2 system to ensure no major issues are present before the test is run in full.

3 Following this, melting is started and a second expansion (Expansion 1) is performed when

4 around 0.5cm of water is present in the bottom of the vessel. This expansion occurred about 35

5 minutes after Expansion 0, with the next expansion (Expansion 2) occurring about 20 minutes

6 later, just before melting finishes, at about the time the ice bath is applied to the vessel. The last

7 three expansions (Expansions 3-5) take place about 30, 60 and 120 min after melting is complete.

8 Expansions 0-5 are reported along a time scale on Fig.3 of the manuscript.

9 **1.9.3. Types of Tests and Data Corrections**

10 To account for the procedural CO blank of the extraction line, two types of tests were performed.

11 The first is the "No-Melt" test, where the procedure is as described above except that the ice

12 sample is not melted but kept at -15°C the entire time. The average blank from all No-Melt

13 extractions was 3.2±1.7 ppbv. The second run type is the "Melt" test, involving the full procedure

14 (including melting) described above. In many cases (Table S4), the No-Melt test was performed

15 immediately prior to a Melt test on the same sample. The No-Melt test [CO] values were

16 subtracted from the Melt test [CO] values to isolate the effect of the melting step on [CO]. When

17 a No-Melt test was not available for a given sample, the average of No-Melt tests run in a similar

18 fashion to the Melt test was used to subtract the extraction line [CO] blank.

19 The rate at which sample aliquots were expanded out of the vessel ("slow expansion" or "fast

20 expansion"; Table S4) was reduced approximately in the middle of this set of tests, as it was

21 determined that faster expansion may have allowed some water vapor to break through the

22 cryogenic trap, potentially causing an elevated response in the RGD detector (higher [CO]). The

23 results of the tests conducted using fast expansions were further corrected for this effect (1.9

24 ppbv), based on a comparison of tests run on depth-replicate firn samples using fast versus slow

25 expansions.

26 The amount of excess CO produced from melting was calculated by subtracting the starting CO

27 concentration before melting (expansion 0) from the final CO concentration after melting

28 (averaging expansions 2-5). When the starting value (expansion 0) was not available (n=2), an

29 average of starting values (expansion 0) from similar runs was used instead. This "excess CO"

30 represents our best estimate of CO increase that is attributable solely to the melting step.

1   Finally, replicate firn samples run in "solid" and "powder" modes showed similar results (Table
2   S4), allowing to ensure that the extra sample processing (grating step) needed for ice samples
3   did not result in excess and variable CO production in the ice samples.

Sample Reference	Top Depth (m)	Bottom Depth (m)	Powder Test ?	Melt Time (Minutes)	Sample Size (kg)	Standard Gas added (cc STP)	TOC (ppbC)	Continuous [CO] (ppbv)	Excess CO, discrete analyses (ppbv)
Gas Free Ice	-	-	Yes	30	0.743	226.2	≤ 2.0	n.d.	9.3
Central Greenland Firn 1-A	45.10	45.30	No	78	1.089	191.4	n.d.	n.d.	7.6
Central Greenland Firn 1-B	45.10	45.30	No	76	0.92	191.9	n.d.	n.d.	9.9
Central Greenland Firn 1-C	45.10	45.30	No	42	0.813	200.0	n.d.	n.d.	7.5
Central Greenland Firn1- D	45.10	45.30	No	48	1.015	197.4	n.d.	n.d.	6.1
Central Greenland Firn 2-A	44.89	45.06	No	61	0.935	209.4	n.d.	n.d.	5.8
Central Greenland Firn 2-B	44.89	45.06	No	45	0.819	222.6	n.d.	n.d.	3.7
Central Greenland Firn 2-C	44.89	45.06	Yes	43.5	0.66	237.6	n.d.	n.d.	7.8
Central Greenland Firn 2-D	44.89	45.06	Yes	39	0.788	222.0	n.d.	n.d.	5.8
Central Greenland Firn 3-A	44.72	44.89	No	44	0.809	219.9	n.d.	n.d.	5.9
Central Greenland Firn 3-B	44.72	44.89	Yes	33	0.678	232.0	n.d.	n.d.	2.4
Central Greenland Firn 3-Small-A	44.72	44.80	No	33	0.379	189.5	n.d.	n.d.	5.4
Central Greenland Firn 3-Small-B	44.63	44.71	No	28.5	0.272	192.5	n.d.	n.d.	4.7
Central Greenland Firn 3-Small-C	44.72	44.80	No	34.5	0.298	198.1	n.d.	n.d.	4.2
Central Greenland Firn 3-Small-D	44.63	44.71	No	27	0.3	196.1	n.d.	n.d.	4.7
PLACE ice: elevated CFA [CO]-A	110.69	110.48	Yes	30	0.793	197.8	26.0	186.3 ± 27.7	7.2
PLACE ice: elevated CFA [CO]-B	110.69	110.48	Yes	48	0.682	212.7	26.0	186.3 ± 27.7	6.6
PLACE ice: low CFA [CO]-A	109.76	109.69	Yes	26	0.604	201.3	18.4	128.7 ± 10.6	3.6
PLACE ice: low CFA [CO]-B	109.69	109.52	Yes	43	0.661	212.4	16.0	129.7 ± 8.0	4.3
Taylor Glacier (Antarctica, 15 kyrs old)	≈6	-	Yes	41	0.626	237.8	n.d.	n.d.	6.2
Taylor Glacier (Antarctica, 6 kyrs old)	≈6	-	Yes	28.5	0.674	210.6	n.d.	n.d.	8.3

Table S4. Sample information for tests used to investigate the hypothesis of rapid CO production from trace organics in the ice during ice melting. Firn samples were all taken from a firn core from Summit, Central Greenland (camp C14), and are denoted by a number and letter combination; the number is the depth level (1-3) and the letters are the replicate sample (A-D) from that level. The "Small" Firn samples came from Firn block 3-C and Firn block 3-D, which were cut in half to create "Small" Firn samples A-D. PLACE ice samples follow a similar naming scheme, with the number representing the depth level and the letter indicating the replicate sample. The "PLACE ice: low CFA [CO]" samples were selected from two distinct sections of the PLACE core that displayed a minimal amount of the high frequency variation in the CFA CO record, with no large CO peaks observed, whereas the "PLACE ice: elevated CFA [CO]" samples were taken from a region with a large amount of the high frequency variation in the CFA CO record and large CO peaks observed. Sample ice from Taylor Glacier (Antarctica) was used and is labeled by age of the ice as only a single sample of each was run. Lastly, "Gas Free Ice" was produced in the laboratory and used as a control sample. The "Excess CO" reported in the table is the average of Expansion 2-5 for a given sample and has been blank corrected.

2. Continuous CO dataset

2.1. Revisiting NEEM-2011-S1 CO data calibration

For the first time, continuous [CO] was collected along the NEEM-2011-S1 core at DRI, in 2011 (Faïn et al., 2014), by coupling a continuous melting setup with a laser (OF-CEAS) spectrometer. While this analytical setup generated stable measurements of CO concentrations with an external precision of 7.8 ppbv (1σ), it suffered from a poor accuracy. Absolute calibration of the NEEM-2011-S1 dataset could not be established by Faïn et al. (2014).

In the framework of this study, we had the opportunity to analyze samples from the NEEM-SC core. These NEEM-SC samples showed a 10 m overlap in depth with the NEEM-2011-S1 record (overlap spanning 399–409 m depth), and then extended deeper. It was of high interest to reevaluate the CFA-based calibration of the NEEM-2011-S1 core so as to obtain a coherent NEEM composite record.

During the NEEM-2011-S1 campaign, for the first time we attempted to use a calibration loop to evaluate (i) blank, and (ii) solubility of continuous CO data. However, the CL did not work properly, resulting in a highly uncertain CO blank (48±25 ppbv), and no internal calibration. Here, we reprocessed the NEEM-2011-S1 CO data using the CO blank and internal calibration established for the NEEM-SC core analyzed 2013 (35±7 ppbv, and 0.96 solubility correction). A fraction of the NEEM-SC core (depth intervals: 573–491m and 444–399 m) was indeed analyzed with a CFA system similar to the one set up in 2011 for the NEEM-2011-S1 core.

Figure S12 shows the good agreement when NEEM-2011-S1 reprocessed data and the NEEM-SC data overlap over the 399-409 m interval. Such good agreement did not exist when using the NEEM-2011-S1 data as initially processed by Faïn et al. (2014).
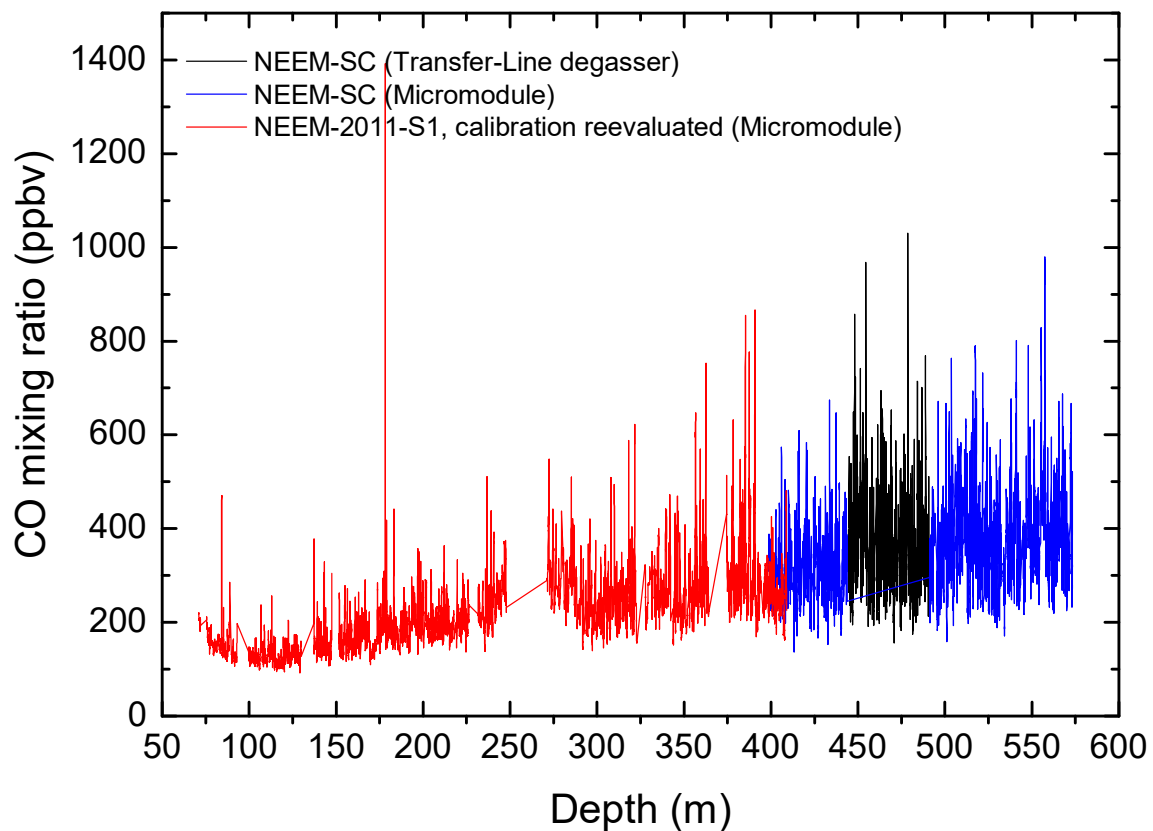
Figure S14. Continuous CO dataset measured on two different cores collected at the NEEM site: the NEEM-2011-S1 core, and the NEEM deep core (SC archive section). NEEM-2011-S1 and NEEM-SC dataset overlap over the 399-409 m interval. The NEEM-2011-S1 core calibration has been revised in the frame of this study. The NEEM-2011-S1 was analyzed with a Micromodule degasser. The NEEM-SC core was analyzed with either a Transfer-Line or a Micromodule degasser.

2.2. Full Continuous CO records

Figure S15 reports the full continuous [CO] records measured along the ice cores investigated in this study: Tunu13, D4, NEEM (SC and 2011-S1 combined), PLACE (DRI) and NGRIP.
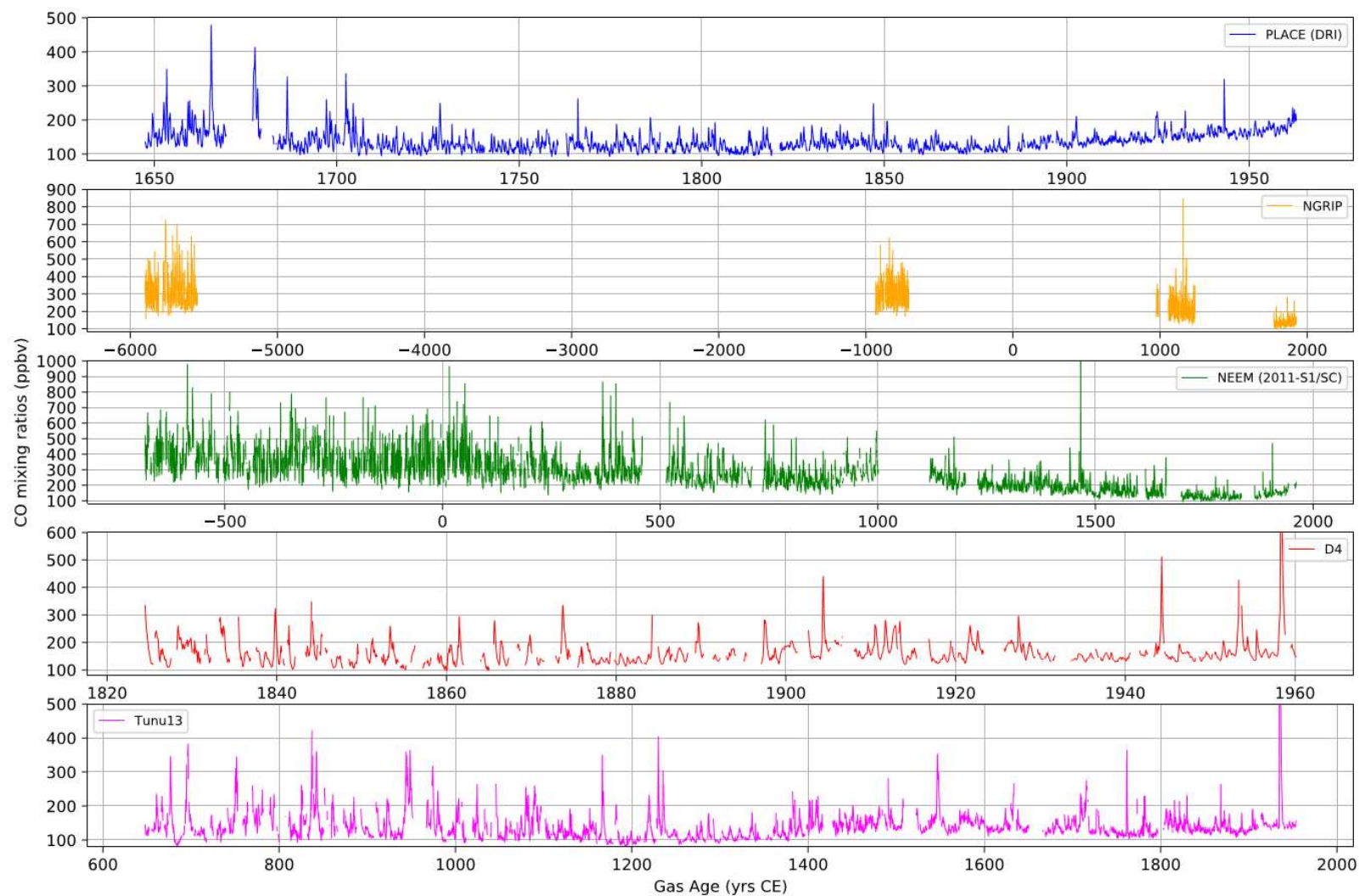
Figure S15. Full continuous [CO] dataset for the Place (DRI), NGRIP, NEEM (combining NEEM-2011-S1 and NEEM-SC cores), D4, and Tunu13 ice cores.

2.3. Comparing DRI and IGE PLACE continuous CO records

In the framework of this study, the PLACE core was analysed for continuous, high resolution, CO mixing ratio with both the DRI (USA) and IGE (France) CFA setups (Table S2). The PLACE core was drilled in June 2015, and analysed at DRI in September 2015. The CFA-based CO measurements were conducted at IGE 18 months later, in February 2017. The PLACE core was stored at <-20°C at NICL prior to being shipped to France. During the shipment, the ice remained at <-20°C.

Figure S16 reports both DRI and IGE continuous CO datasets. The two records are extremely similar in the 115-153 m depth interval. However, DRI and IGE CO records exhibit differences in the 80-115 m depth interval: while CO spikes are located at the same depths in the IGE and DRI records (e.g., Fig.2 of the manuscript), their amplitudes are larger in the IGE record.
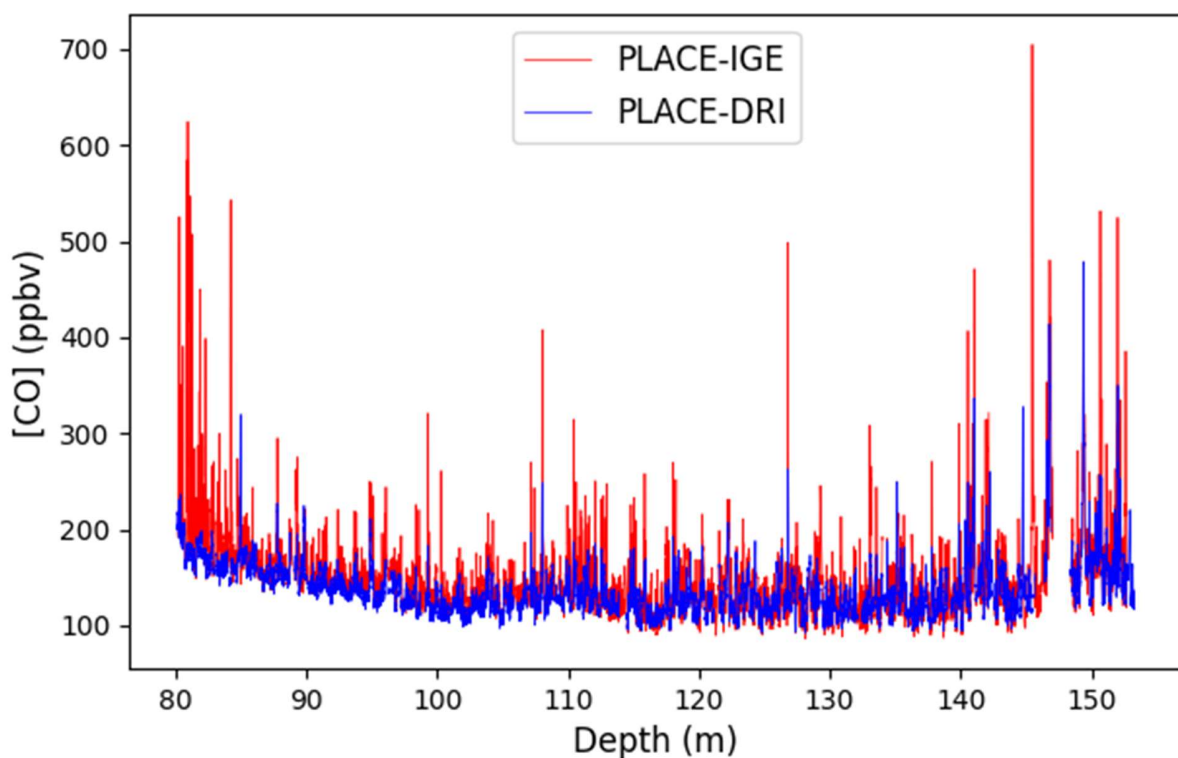

Figure S16. PLACE continuous CO records collected on the DRI and IGE CFA setups in September 2015 and February 2017, respectively.

Figure S17 compares mean and 5th percentile (i.e., baseline) CO extracted from the DRI and IGE high resolution datasets. Mean and 5th percentile of the data are calculated every 4 years over a

29

1   moving window of 15 yrs. Shaded envelopes reported in Fig. S17 represent the uncertainties (1σ).

2   The PLACE CO baseline extracted from the IGE continuous record is similar to the one based on

3   the DRI dataset: both baselines agree within their uncertainty envelopes. Replicate datasets (Fig.

4   S3) further rule out analytical drifts of the DRI or IGE CO baselines during the measurements: in

5   both laboratories, we first melted the entire core, and later some replicate sections were

6   reanalyzed. Such replicate measurements exhibit an excellent agreement with the main records

7   (Fig. S3).
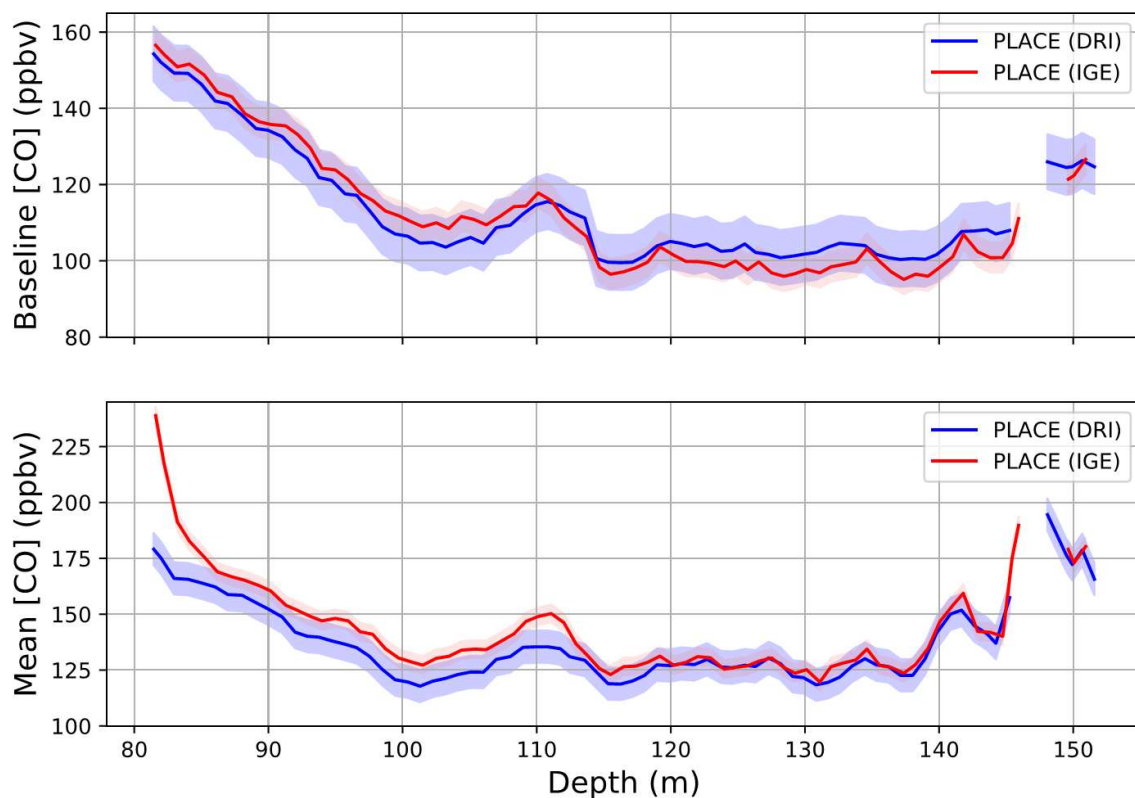
9   **Figure S17.** Comparison of means and 5th percentiles (i.e., baseline) CO signals extracted from the

10   continuous CO records measured on the DRI and IGE CFA setups. Shaded envelopes represent the

11   uncertainties.

12

13   The PLACE mean CO mixing ratios measured at DRI and IGE are in excellent agreement along

14   the 115-153 m depth interval (Fig. S17). However, mean CO mixing ratios measured at IGE are

15   ~10 ppbv higher than the DRI levels in the 85-115 m depth range, and much higher in the 80-85

16   m depth interval. In the 80-85 m depth interval, we hypothesize that post-coring entrapment of

modern air (e.g., Aydin et al., 2012) during the 18 months storage prior to the IGE analytical campaign can explain [CO] enhancement observed on the IGE record.

The reason for why the 85-115 m depth interval of the IGE CO record exhibits higher mean and CO spikes (but similar CO baseline) remains unexplained. We do not expect that the 18 months storage period between DRI and IGE PLACE analytical campaigns would impact CO patterns, as indicated by replicate measurements made 22 months apart (Fig. S12). Laboratory investigations conducted on discrete samples support the idea that the elevated and highly variable [CO] values observed in Greenland ice samples are due to excess CO produced from in situ production within the ice itself rather than extraneous CO production during ice melting (Sect. 3.2.4), and this conclusion should apply to both DRI and IGE CFA setups. Further, offsets between the IGE and DRI records caused by procedural artifacts would be expected to affect the entire record, not just the parts of the cores shallower than 115 m. One possibility may be that the post-coring air trapping effect is important to depths greater than 85 m. Relative air content measurements by Kobashi et al. (2010) suggested that there may still be pockets of interconnected open porosity as deep as ≈130 m at Greenland Summit, and this could in principle result in relatively higher CO observed in IGE measurements.

Overall, the difference between continuous CO records collected at DRI and IGE remains small, with a gap in mean levels never exceeding 10 ppbv for ice sections which are not near the firn-ice transition, and this offset does not affect our conclusions regarding baseline CO trends.

3. Chemistry dataset and analyses

3.1. High resolution TOC datasets

High resolution, continuous TOC datasets collected at DRI are reported for the PLACE core (Fig. S18) and the Tunu13 core (Fig. S19).
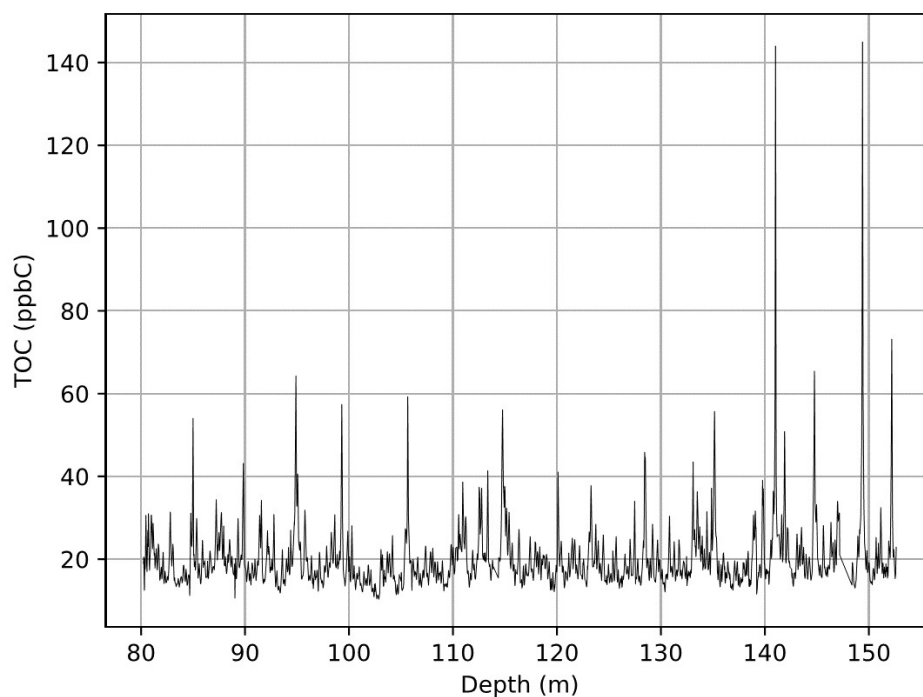
1

2   **Figure S18.** High resolution, continuous TOC dataset collected along the PLACE core with the DRI CFA
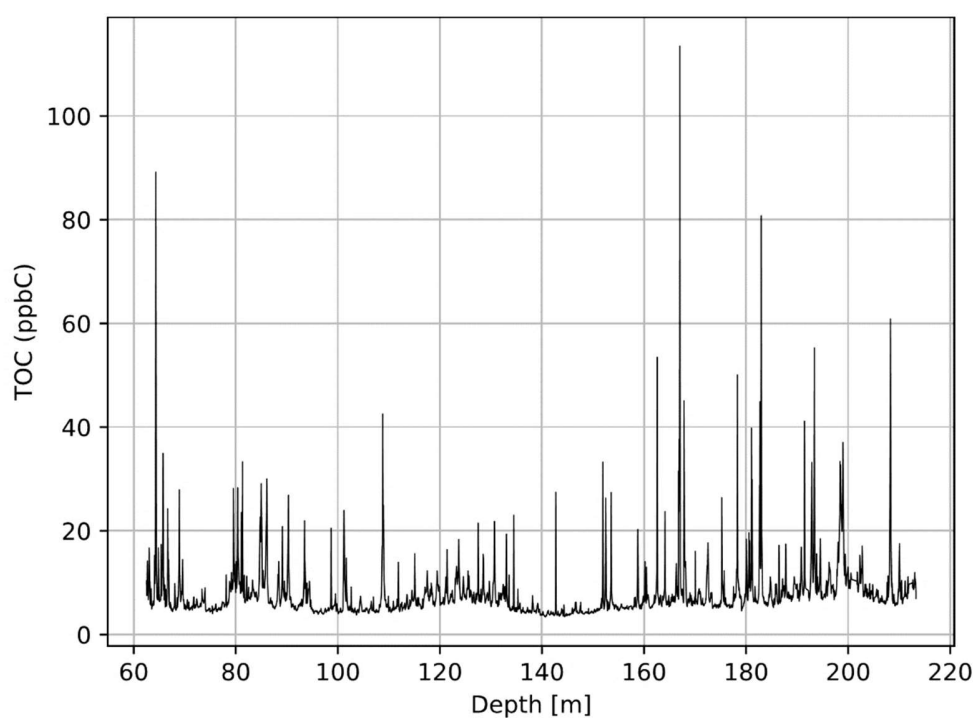
3   setup.

4   .

5   **Figure S19.** High resolution, continuous TOC dataset collected along the Tunu13 core with the DRI CFA

6   setup.

1 ### 3.2. Relationship between TOC and Accumulation at Tunu13

2 Figure S20 reports the relationships between TOC and surface snow accumulation rate Tunu13.
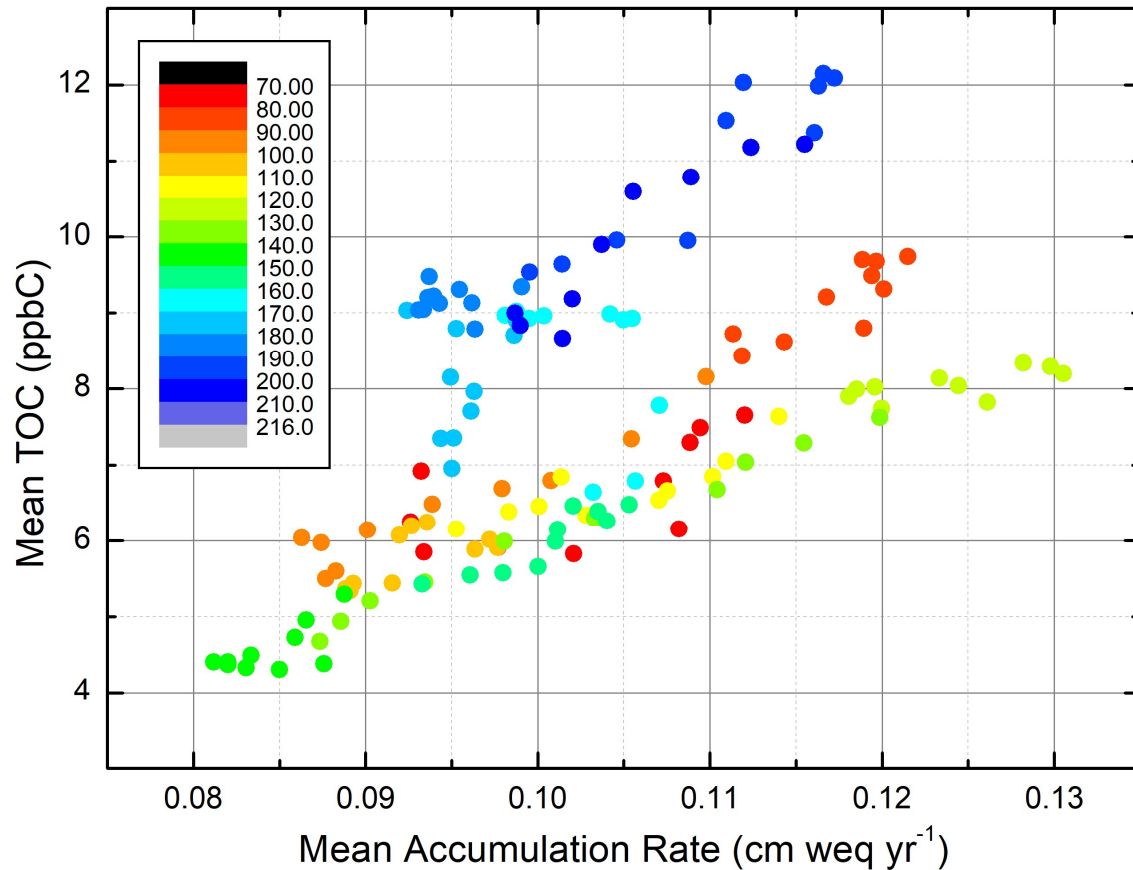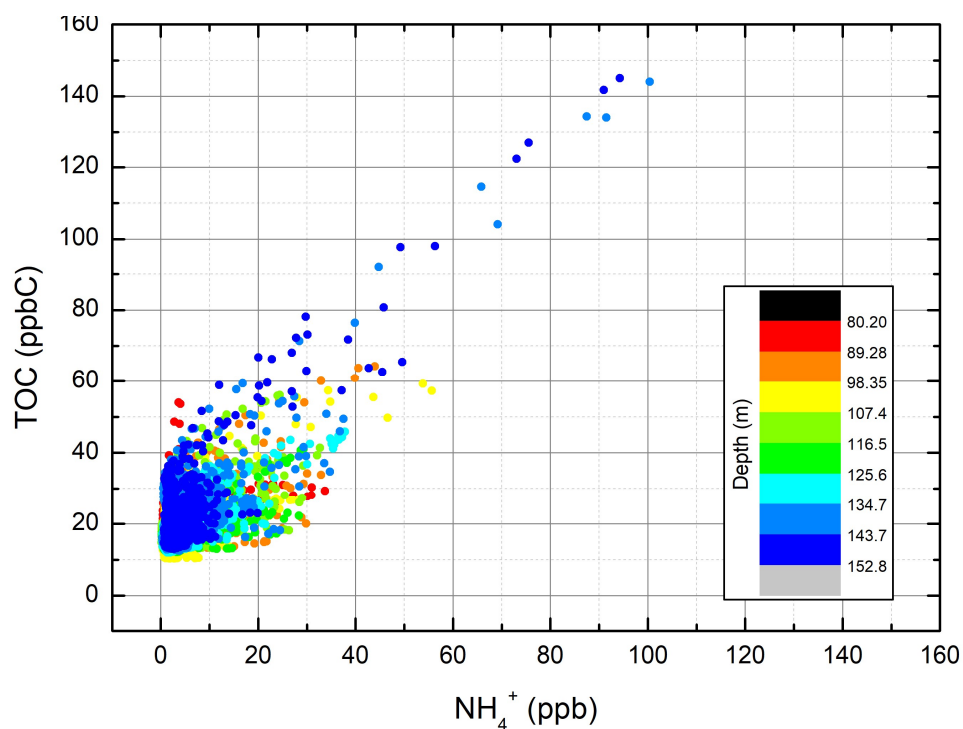

3

4 **Figure S20.** TOC vs Accumulation rate (annually averaged dataset) plotted for the Tunu13 ice core. The
5 color scale reports the depth, varying from 78 to 216 m depth.

6

7

8 ### 3.3. Relationship between TOC and ammonium at Tunu13 and PLACE

9 Figures S21 and S22 report the relationships between TOC and ammonium at PLACE and
10 Tunu13, respectively.

11

1

2 **Figure S21.** Relationship between TOC and ammonium for the PLACE ice core. The slope is close to unity.

3 The color scale indicates depth in meters.
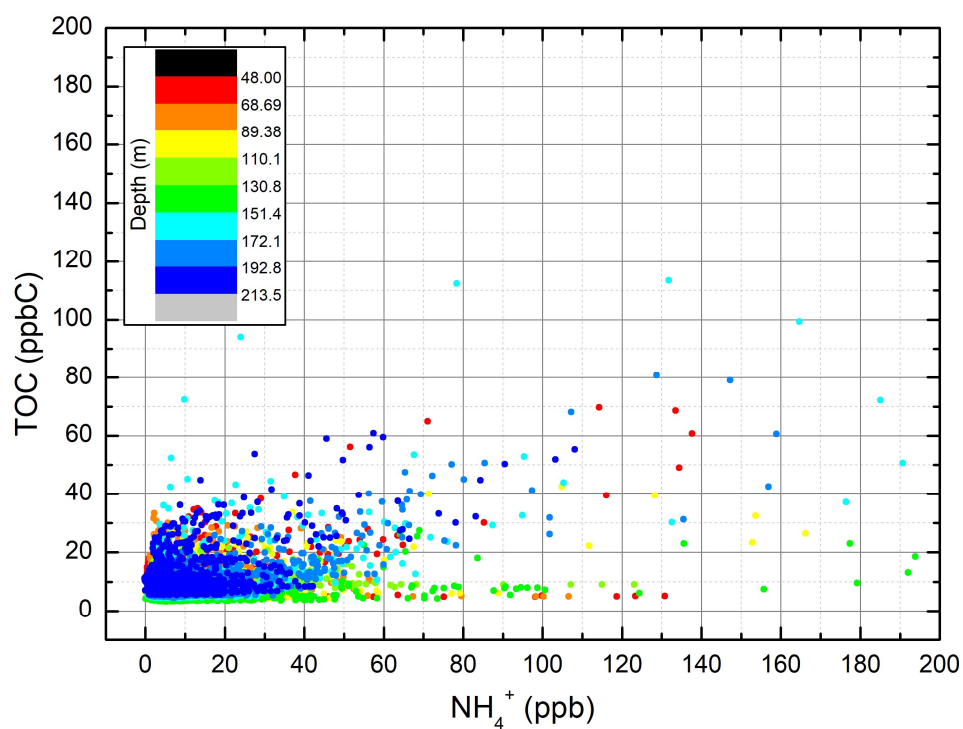
4

5 **Figure S22.** Relationship between TOC and ammonium for the Tunu13 ice core. Unexpectedly low TOC

6 is observed along ammonium peaks. The color scale indicates depth in meters.

1   ### 3.3. High resolution H_2O_2 dataset

2   High resolution, continuous H_2O_2 datasets collected at DRI are reported for the PLACE and
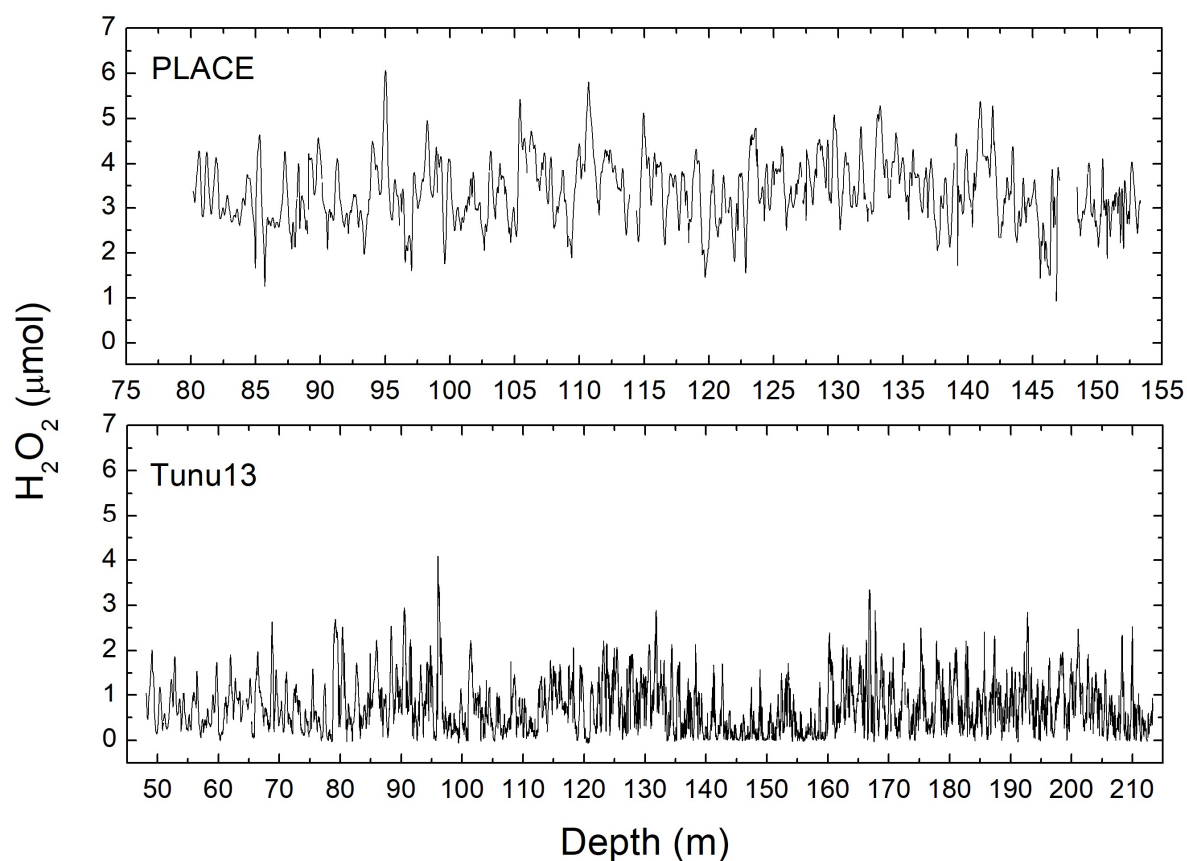
3   Tunu13 ice cores (Fig. S23).

4

5   **Figure S23.** High resolution, continuous H_2O_2 datasets collected along the PLACE (upper panel) and

6   Tunu13 (lower panel) ice cores with the DRI CFA setup.

4. References

Allan, D. W.: Statistics of atomic frequency standards, Proc. IEEE, 54(2), 221–230, doi:10.1109/PROC.1966.4634, 1966.

Aydin, M., Montzka, S. A., Battle, M. O., Williams, M. B., De Bruyn, W. J., Butler, J. H., Verhulst, K. R., Tatum, C., Gun, B. K., Plotkin, D. A., Hall, B. D. and Saltzman, E. S.: Post-coring entrapment of modern air in some shallow ice cores collected near the firn-ice transition: evidence from CFC-12 measurements in Antarctic firn air and ice cores, Atmos. Chem. Phys., 10(11), 5135–5144, doi:10.5194/acp-10-5135-2010, 2010.

Bigler, M., Svensson, A., Kettner, E., Vallelonga, P., Nielsen, M. E., Steffensen, J. P. and Peder, J.: Optimization of High-Resolution Continuous Flow Analysis for Transient Climate Signals in Ice Cores, Environ. Sci. Technol., 45(10), 4483–4489, doi:10.1021/es200118j, 2011.

Buizert, C., Martinerie, P., Petrenko, V. V., Severinghaus, J. P., Trudinger, C. M., Witrant, E., Rosen, J. L., Orsi, A. J., Rubino, M., Etheridge, D. M., Steele, L. P., Hogan, C., Laube, J. C., Sturges, W. T., Levchenko, V. A., Smith, A. M., Levin, I., Conway, T. J., Dlugokencky, E. J., Lang, P. M., Kawamura, K., Jenk, T. M., White, J. W. C., Sowers, T., Schwander, J. and Blunier, T.: Corrigendum to "Gas transport in firn: multiple-tracer characterisation and model intercomparison for NEEM, Northern Greenland'" published in Atmos. Chem. Phys., 12, 4259–-4277, 2012", Atmos. Chem. Phys., 14(7), 3571–3572, doi:10.5194/acp-14-3571-2014, 2014.

Faïn, X., Chappellaz, J., Rhodes, R. H., Stowasser, C., Blunier, T., McConnell, J. R., Brook, E. J., Preunkert, S., Legrand, M., Debois, T. and Romanini, D.: High resolution measurements of carbon monoxide along a late Holocene Greenland ice core: evidence for in situ production, Clim. Past, 10(3), 987–1000, doi:10.5194/cp-10-987-2014, 2014.

Fourteau, K., Faïn, X., Martinerie, P., Landais, A., Ekaykin, A. A., Lipenkov, V. Y. and Chappellaz, J.: Analytical constraints on layered gas trapping and smoothing of atmospheric variability in ice under low-accumulation conditions, Clim. Past, 13(12), 1815–1830, doi:10.5194/cp-13-1815-2017, 2017.

Kobashi, T., Severinghaus, J. P., Barnola, J. M., Kawamura, K., Carter, T. and Nakaegawa, T.: Persistent multi-decadal Greenland temperature fluctuation through the last millennium, Clim. Change, doi:10.1007/s10584-009-9689-9, 2010.

MacFarling Meure, C., Etheridge, D. M., Trudinger, C. M., Steele, P., Langenfelds, R., van Ommen, T., Smith, A. and Elkins, J.: Law Dome CO_2, CH_4 and N_2O ice core records extended to 2000 years BP, Geophys. Res. Lett., 33(14), doi:Artn L14810 doi 10.1029/2006gl026152, 2006.

McConnell, J. R., Lamorey, S. W. and Taylor, K. C.: Continuous ice-core chemical analyses using inductively coupled plasma mass spectrometry, Environ. Sci. Technol., 36(1), 7–11, 2002.

Mitchell, L. E., Brook, E. J., Lee, J. E., Buizert, C. and Sowers, T.: Constraints on the late holocene anthropogenic contribution to the atmospheric methane budget., Science (80)., 342(6161), 964–6, doi:10.1126/science.1238920, 2013.

Morville, J., Kassi, S., Chenevier, M. and Romanini, D.: Fast, low-noise, mode-by-mode, cavity-enhanced absorption spectroscopy by diode-laser self-locking, Appl. Phys. B-Lasers Opt., 80(8), 1027–1038, doi:10.1007/s00340-005-1828-z, 2005.

Rasmussen, S. O., Abbott, P. M., Blunier, T., Bourne, A. J., Brook, E. J., Buchardt, S. L., Buizert, C., Chappellaz, J., Clausen, H. B., Cook, E., Dahl-Jensen, D., Davies, S. M., Guillevic, M., Kipfstuhl, S., Laepple, T., Seierstad, I. K., Severinghaus, J. P., Steffensen, J. P., Stowasser, C., Svensson, A., Vallelonga, P., Vinther, B. M., Wilhelms, F. and Winstrup, M.: A first chronology for the North Greenland Eemian Ice Drilling (NEEM) ice core, Clim. Past, 9(6), 2713–2730, doi:10.5194/cp-9-2713-2013, 2013.

Rhodes, R. H., Faïn, X., Stowasser, C., Blunier, T., Chappellaz, J., McConnell, J. R., Romanini, D., Mitchell, L. E. and Brook, E. J.: Continuous methane measurements from a late Holocene Greenland ice core: Atmospheric and in-situ signals, Earth Planet. Sci. Lett., 368, 9–19, doi:10.1016/j.epsl.2013.02.034, 2013.

Rhodes, R. H., Faïn, X., Brook, E. J., McConnell, J. R., Maselli, O. J., Sigl, M., Edwards, J. S., Buizert, C., Blunier, T., Chappellaz, J. and Freitag, J.: Local artifacts in ice core methane records caused by layered bubble trapping and in situ production: a multi-site investigation, Clim. Past, 12(4), 1061–1077, doi:10.5194/cp-12-1061-2016, 2016.

Rosen, J. L., Brook, E. J., Severinghaus, J. P., Blunier, T., Mitchell, L. E., Lee, J. E., Edwards, J. S. and Gkinis, V.: An ice core record of near-synchronous global climate changes at the Bølling transition, Nat. Geosci., 7(6), 459–463, doi:10.1038/ngeo2147, 2014.

Sigl, M., Winstrup, M., McConnell, J. R., Welten, K. C., Plunkett, G., Ludlow, F., Büntgen, U., Caffee, M., Chellman, N., Dahl-Jensen, D., Fischer, H., Kipfstuhl, S., Kostick, C., Maselli, O. J., Mekhaldi, F., Mulvaney, R., Muscheler, R., Pasteris, D. R.,Stowasser, C., Buizert, C., Gkinis, V., Chappellaz, J., Schüpbach, S., Bigler, M., Faïn, X., Sperlich, P., Baumgartner, M., Schilt, a., Blunier, T. and Schupbach, S.: Continuous measurements of methane mixing ratios from ice cores, Atmos. Meas. Tech., 5(5), 999–1013, doi:10.5194/amt-5-999-2012, 2012.

1   Stowasser, C., Buizert, C., Gkinis, V., Chappellaz, J., Schüpbach, S., Bigler, M., Faïn, X., Sperlich,

2   P., Baumgartner, M., Schilt, a., Blunier, T. and Schupbach, S.: Continuous measurements of

3   methane mixing ratios from ice cores, Atmos. Meas. Tech., 5(5), 999–1013, doi:10.5194/amt-5-

4   999-2012, 2012.